AALBORG UNIVERSITET
STUDENTERRAPPORT

10th semester at
The Faculty of Engineering and Science
Energy Technology
Pontoppidanstræde 111
9220 Aalborg

Title:

Modelling of biomass combustion and ash deposition in an 88 MW grate-fired boiler

Project:

Master thesis

Project period:

Autumn 2020

Author:

Shakerullah Nazari

Supervisor:

Chungen Yin

Number of pages: 36
Deadline: 31-10-2020

Resumé

Dette projekt omhandler modellering af forbrænding og askedannelse i en 88 MW ristfyret biomasse kedel(EV3). Fremgangsmåden for modelleringsdelen er i to dele: en empirisk model for de termo-kemiske processer, der finder sted ved risten når biomassen bliver transporteret til forbrændingskammeret, og en forbrædningsmodel der beskriver selve forbrændingen i forbrændingskammeret. Modellen for de termo-kemiske processer ved risten er baseret på antaget konverteringsrater langs risten ud fra målinger og erfaringer. Dermed beregner denne model temperaturen, hastigheden og kompositionen af brændselsgassen, der forlader risten og indtræder i selve forbændingskammeret. Temperaturen, hastigheden og kompositionen bliver brugt som randbetingelser for selve forbrændingsprocessen i kammeret sammen med randbetingelser for andre flader. I selve forbrændingskammeret bliver forbrændingsmodeller samt strålingsmodeller brugt til at beregne forløbet i brændselskammeret.
Desuden, kobles simuleringerne for forbrænding sammen med en askedannelses model, som er en iterativ model, der beregner tykkelsen af asken på blandt andet varmevekslerne. Resultaterne fra simuleringerne er sammenholdt med målinger. Disse sammenligninger viser, at der er en relativ betydningsfuld afvigelse mellem resultaterne fra modellen og målingerne. Hovedårsagen til disse afvigelser er, at modellen er baseret på en hel ren kedel, hvorimod målinger er fortaget af kedlen i drift. Af denne årsag, er randbetingelser brugt i simulering af forbrændingen muligvis ikke identiske med de faktiske randbetingelser. Desuden, er der i modellen heller ikke taget højde for askedannelsen, da simuleringerne er stationær tilstand simuleringer. Kontur-billederne af selve forbrændingen i kedlen viser at der er to lokale recirkulations zoner i forbrændingskammeret, hvorfor sammenblanding mellem forbrændingsgassen og sekundær ilt, der tilføres gennem dyserne, må være god. Askedannelsesmodellen fungerede ikke som planlagt, og deraf ingen askedannelses resultater for kedlen EV3. Men den samme askedannelses model har Chungen Yin, lavet simuleringer med på en anden kedel, og disse simuleringer blev stillet til rådighed. Resultaterne af disse simuleringer er forarbejdet, og disse viser, at askedannelsen i kedlen har en betydelig effekt på hjørnerne af varmevekslerne. Temperaturen på varmevekslernes hjørner er højere end andre steder kvag askedannelsen.

Preface

The use of biomass for heat and power production increases due to the global discourse of transition of the energy sector to renewable energy sources. Thus, this master thesis serves as a contribution to improve our understanding of biomass combustion. It is written as a part of the Master of Science Programme for the Thermal Energy and Process Engineering study at Aalborg University.

Reading Guide
To make the reading more comprehensive all equations, tables and figures have been numbered to the corresponding chapter they appear in. For example, the second figure in Chapter 3, is numbered 3.2.In addition, with every figure and table a brief explanation in the caption is presented.

Variables and abbreviations that have been used in equations are placed in a separate nomenclature at the beginning of the report. The first time an abbreviation of a name or a concept appear in the text, it will be written in full followed by its abbreviation in parenthesis.

For citations, the Harvard Method has been used. This means that the author's surname, or name of a website if no author has been cited, and year of publication will appear as notes in the text. The notes are only a reference to the complete bibliography at the end of the report. Websites are listed with author, title, URL and date, while books are listed with tittle, year,publisher and ISBN.

Appendices are placed at the end of the report (if any) and are denoted A, B and so on.

All simulations are performed using ANSYS® Academic Fluent®, Release 19.2.

I want to thank Chungen Yin for his support and supervision.

Nomenclature

Symbol	Description	Unit
$\dot{m}''_{d,kcl,vapor}$	Total deposition of Kcl	$Kg/m^2 \cdot s$
u_d^+	Dimensionless deposition velocity	m/s
u_d	Deposition velocity	m/s
u_τ	Friction velocity	m/s
$\dot{m}''_d$	Particle deposition flux	$kg/m^2 \cdot s)$
C_o	Near wall particle mass concentration	kg/m^3
τ_w	Wall shear stress	$kg/m \cdot s^2$
$u^+_{d,Diff}$	Diffusion regime	$[-]$
$u^+_{d,Turb}$	Turbulent regime	$[-]$
Sc_p	Particle Schimdt number	$[-]$
K_B	Boltzmann's constant	J/K
C_c	Cunningham slip correction	$[-]$
Y	Mean free path of gas	m
ν	Kinematic viscosity	m^2/s
τ_p^+	Dimensionless particle relaxation time	$[-]$
S	particle to gas density ratio	$[-]$
d_p^+	Dimensionless particle size	$[-]$
$u^+_{d,Therm}$	Dimensionless particle deposition velocity due to thermophoresis	$[-]$
m_p	Particle mass	kg
τ_p	Particle relaxation time	s
F_{therm}	Thermophoretic force	N
K_n	Knudsen number	$[-]$
$\dot{m}''_{d,Dpm}$	Total deposition of fly ash	$[-]$
$\dot{m}_p$	Flow rate of particle being treated that is currently hitting a wall	Kg/s
$Conc_p$	Particle mass concentration	Kg/m^3
η_{stick}	Net fraction of particles contributing to deposit growth	$[-]$
f_{melt}	Melt fraction	$[-]$
M	Mass pr.atom	kg/atom
C_v	Specific heat	J/(kg-k)
R	Gas constant	J/(Kg-K)
d_m	Molecular diameter	m
∇T	Temperature gradient	K/M
$qconv$	Convective heat	w
K_{gas}	Heat transform coefficient	$w/(m-k)$
A_{conv}	Area	m^2
T_g	Gas temperature	K
A	Area of the reflecting surface that the particle is hitting	m^2
ρ	Gas Density Near Wall Cell	Kg/m^3

Acronyms, special symbols and denotations

Acronym	Description
AAU	Aalborg University
UDF	User Defined Functions
CFD	Computational Fluid Dynamics
EBU	Eddy Break-Up
EDM	Eddy Dissipation Model
MW	Mega Watt
RTE	Radio Transfer Equations
DOM	Discrete ordinate Models
DNS	Direct Numerical Simulation
LES	Large Eddy Simulation
RANS	Reynolds- Averaged-Navier-Stokes (RANS)
SA	Secondary Air
OFA	Overfire Air
PA	Primary Air
LHV	Lower Heat Value
BC	Boundary Condition
DIFF	Diffusion
TURB	Turbulent
THERM	Thermophoresis
CONC	Concentration
CONV	Convection

Table of contents

Introduction 1

The global concern about ensuring an environmental-friendly and sustainable energy sector has made the interest for renewable energy sources increase. Most of the countries have political agendas to reduce or phase out the use of fossil fuels in the energy sector. The EU agreed on energy and climate targets to be achieved before 2030 and some of the objectives are to reduce the greenhouse gas emissions by at least 40% compared to 1990 and to at least use 27 % of renewable energy sources in the final energy consumption. Biomass is considered to be an important energy source for achieving the goals set by the EU and other energy sectors throughout the world. In the past two decades, the use of Biomass for energy production has rapidly increased in many countries in the world and the increase is expected to continue [Dörrenbächer et al., 2017]. Biomass combustion technologies are responsible for over 90 % of the global contribution to bioenergy[Koppejan and van Loo, 2008]. Therefore, it is important to understand biomass combustion and the challenges faced with this technology in order to optimize the existing systems.

1.1 Biomass Combustion

Biomass is converted into useful energy by thermochemical- and biochemical conversion technologies. The latter is by fermentation for alcohol production and anaerobic digestion for producing methane-enriched gas. However, in this project only the thermochemical conversion technologies are considered. The main thermochemical technologies used for biomass conversion are illustrated in Figure 1.1. The technologies are in various stage of development. The most commonly used and developed is combustion. The process of combustion can generally be divided into several processes i.e.drying, pyrolysis, gasification and combustion. The combustion process can either be continuous or batch combustion, and the air supply can either be forced or natural depending on the application and fuel properties. Industrial combustion applications are always continuous with forced draugth.

Drying is carried out to evaporate moisture from the fuel used for combustion at low temperatures. Moisture content of the fuel is important for the combustion process, since the energy required for drying is released from the combustion process and this reduces the temperature of the combustion chamber. Hence, slowing down the

combustion process.
In pyrolysis, a thermal degradation (devolatilization) of the fuel is taking place without externally supplying an oxidizing agent. Tar, carbonaceous charcoal and low molecular weight gasses are the main products. If the fuel is rich in oxygen, such as biomass, CO and CO_2 are formed in considerable amounts.

Biomass gasification is an incomplete combustion of biomass resulting in gaseous combustbles mainly carbon monoxide and hydrogen. The produced mixtures can be used to run internal combustion engines, methanol production etc.
A complete oxidation of the fuel is called combustion. The products from combustion can be used for heating purposes or electricity production. In a solid-fuel combustion process e.g. biomass combustion, the initial steps will always be drying and pyrolysis/gasification[Koppejan and van Loo, 2008].

Grate-firing is one of the most widely used technologies for biomass combustion due to grate-fired boilers being able to fire a wide range of fuels with varying moisture content. Hence, showing great potential in biomass combustion [Yin et al., 2008c]. Due to the large variation and complicate structure of biomass, the combustion process is complicated. Experimental data collection of grate-fired biomass combustion is difficult and only few investigations are carried out with detailed data collection. For this reason, Computation Fluid Dynamics (CFD) is a strong tool to understand the mechanisms of grate-fired biomass combustion. Numerical CFD simulations of biomass combustion employing complete models for

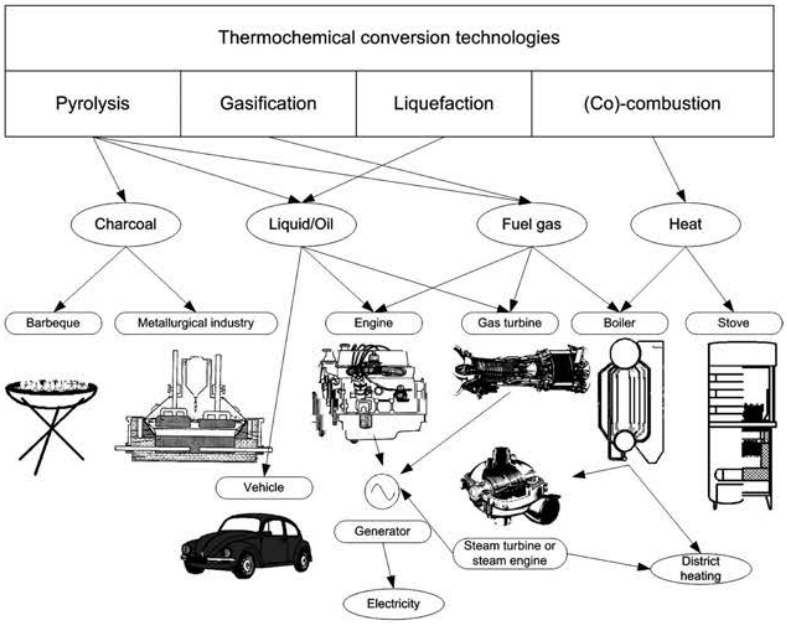

Figure 1.1: *Thermochemical conversion technologies [Koppejan and van Loo, 2008].*

all the difference phases are limited [Karim and Jamal]. However, various approaches have been made focusing on different aspects of grate-fired biomass combustion, as presented in Chapter 2. Even though grate-firing of biomass has been investigated for many years, there are still some challenges to be studied. For instance, the fuel conversion in the fuel bed on the grate, mixing in both the fuel bed and the freeboard, deposit formation and corrosion, numerical simulation to better understand the mechanisms of grate-fired boilers[Yin et al., 2008c].

Thus, the objective of this project is to model a 88 MW grate-fired biomass boiler using CFD and carry out numerical simulations to analyse the combustion in the freeboard, and understand the effect of ash deposition on grate-fired boilers by modelling deposition growth. A state-of-the-art review of the modelling approach of biomass grate-fired boilers will be made. The modelling procedure for the 88 MW grate fired boiler will be explained. The results from the simulation of combustion in the 88MW boiler will be compared to measurements. Finally, temperature, flow and species contours will be analysed to better understand the combustion in the freeboard.

State-Of-The-Art CFD Modelling of Grate-fired Boilers

2

In this chapter, literature on CFD modelling of biomass in grate-fired furnaces is reviewed to understand the modelling aspect of biomass combustion and to develop the modelling approach used in this report. The focus of the chapter is on general CFD modelling approaches, gas phase combustion and radiaton models used in biomass combustion modelling. Furthermore, fuel bed modelling, particle transport and conversion models, and the numerical setup of CFD simulations are investigated.

2.1 General CFD modelling approaches in fixed bed combustion

Fixed bed combustion i.e. grate furnaces are appropriate for fuels with high moisture and ash content, and non-uniform particle sizes. Various types of grate furnaces exists i.e. fixed grates, moving grates, rotating grates and vibrating grates. The technologies are designed for optimal combustion depending on different biomass fuel properties. Three different approaches exist in the literature to model grate furnaces. These are illustrated in Figure 2.1

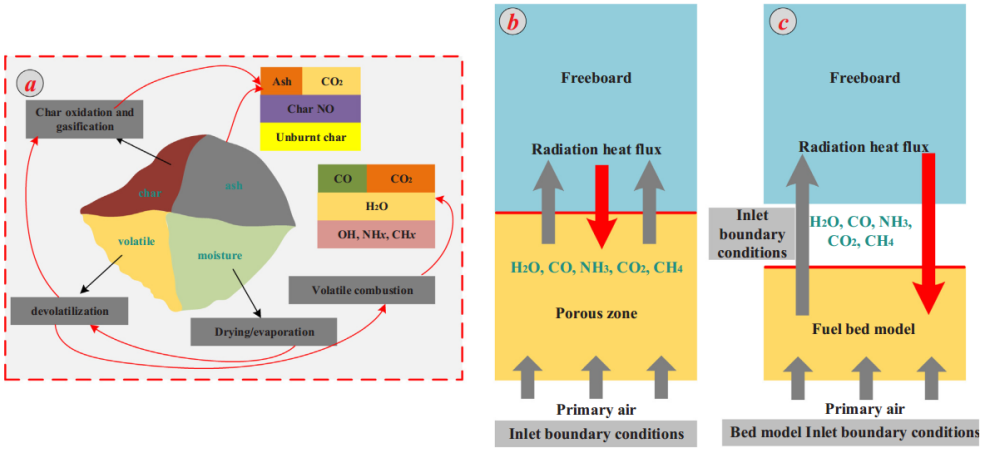

Figure 2.1: *Modelling approaches in grate furnaces [Yongtie et al., 2018]*

The first approach outlined in Figure 2.1 (a) is the empirical modelling. In this modelling approach, the gas phase simulation is provided with inlet boundary conditions such as fuel composition, velocity and temperature calculated from mass and energy balances. These are calculated from the fuel bed by simply dividing the fuel bed into four different sections i.e. drying, devolatilization, char oxidation and ash formation. However, this model cannot predict the gas phase combustion in the design stage[Yongtie et al., 2018].
The second approach (b) in Figure 2.1 is to simultaneously simulate the fuel bed conversion with the gas phase combustion. The fuel bed is treated as a porous medium and a UDF is implemented to depict the thermal conversion in the porous zone. This approach is computationally expensive [Dernbecher et al., 2019].
The third approach 2.1 (c) is the most common approach for biomass combustion i.e. the stand-alone bed model. The fuel bed is separated from the freeboard. In the fuel bed drying, devolatilization, char oxidation is modelled. The resultant gas phase composition, velocity and temperature profiles are used as the inlet boundary conditions for the gas phase combustion. A two way coupling can be implemented so the radiation heat flux from the freeboard onto the fuel bed is accounted for in the fuel bed model [Dernbecher et al., 2019]. Borello et al. [2013] modelled biomass combustion coupled with an ash deposition model based on the stand-alone bed model and CFD combustion in the freeboard. A three phase approach was used i.e. solid-phase combustion in the fuel bed, gas-phase combustion in the freeboard and tracking and deposition of fly ash. The models demonstrated efficient combustion of wood and deposition occured in the expected zones.
Kær et al. [2006] developed a deposition model coupled with a fuel bed conversion model to study the effect of deposition on straw-fired grate boilers. A stand-alone fuel bed conversion model was developed by using the moving column method. Deposition was modelled through a user defined function introduced to the CFD modelling. The models were applied on a straw-fired boiler from Masnedø and the results were in good agreement with the measurements and observations at the plant.
Buczyński et al. [2015] developed a CFD based model to predict the performance of a domestic heating boiler fired with solid fuels. The model was developed by the porous medium approach i.e. the fuel bed and the freebord was modelled as one large domain. The model is used to improve both the design and operation of the boiler. Reshaping the combustion chamber and redirection of the air supply was amongst the suggestions for optimizing the boiler.

2.2 Combustion and radiation models

Combustion models are used to describe the connection between the turbulence and kinetics of chemical reactions in the combustion chamber where mixing of fuel and oxidizer takes place. Various models exist for modelling combustion. However, the models are mainly catagorized into Eddy Break-Up (EBU) models and mixture

fraction models. In the field of biomass combustion modified versions of the EBU models are often used. The EBU model was developed for turbulent premixed flames and it assumes infinitely fast reaction and the velocity is calculated from turbulent mixing. The model was further developed to account for turbulent non-premixed flames and the modified version of the model is the Eddy Dissipation Model (EDM). The finite rate/eddy dissipation model both calculates the Arrhenius rates and the eddy dissipation rates. The minimum value of the former is used.
Literature review on combustion models reveals that the finite rate/eddy dissipation model is used very commonly in biomass combustion. For instance, Galletti et al. [2016a] used the finite rate/eddy dissipation model for combustion to investigate the co-generation of biomass with externally fired gas turbines.
Yin et al. [2008a] used the finit rate/eddy dissipation model for gas-phase combustion in the freeboard in a 108 [MW] grate furnace. The CFD model was developed to have a reliable baseline model for an industrial biomass boiler which can be used for diagnosis and optimization. The default values of the constants A=4 and B=0.5 in the finite rate/ eddy dissipation model overpredicted the temperature peak, thus the constants were refined to A=0.6 and B=0.5 to match the temperature peaks from the measurements. The finite rate/ eddy dissipation amongst other gas-phase combustion requires a definition of the reaction mechanisms.The main reactions in the combustion chamber of biomass combustion are the oxidation of hydrocarbons produced by thermochemical conversion at the fuel bed. These can be modelled as single-step global reaction mechanisms or multi-step reaction mechanisms. The most popular reaction mechanisms is the one proposed by WESTBROOK and DRYER [1981]. It is a two-step oxidation of hydrocarbons with carbon monoxide as the the intermediate. Another well known reaction mechanism, proposed by Jones and Lindstedt [1988], is the four-step reaction mechanism of hydrocarbons with carbon monoxide and hydrogen as the intermediate. Yin et al. [2010] used both of the former two reaction mechanism in modelling co-firing of straw with coal in a swirl-stabilized dual-feed burner. Both combustion models with their respective reaction mechanisms predicted the major chemical species reasonably well.

Radiation in biomass combustion processes is governed by the radiative transfer equations (RTE) ,in which adsorption, emission and scattering of the medium radiation passes through, are accounted for. The most extensively used radiation models in the literature are the Discrete Ordinate Models (DOM). A thorough analysis of radiation models used in biomass combustion was done by Klason et al. [2008]. They concluded that the P1 radiation model achieved fairly good results of simulating radiation in the combustion chamber with less computational effort compared to DOM amongst other. However, the radiative heat flux from the combustion chamber onto the fuel bed was not properly simulated. Therefore, it was suggested not to use the P1 models for biomass combustion problems where the the freeboard gas-phase simulations are coupled with the thermochemical conversion processes at the fuel bed.

2.3 Turbulence modelling

The flow in the freeboard gas-phase combustion is highly turbulent. Mixing of fuel and oxidizer is enhanced by turbulence. Thus, highly turbulent flows are desired in combustion. In the literature various approaches have been made to model turbulence. For instance, Direct Numerical Simulation (DNS), Large Eddy Simulation (LES), and Reynolds-Averaged-Navier-Stokes (RANS) equation. The latter is predominantly used in the field of biomass combustion. Turbulence models are needed to solve the RANS equation and two additional equations are needed to close the system of equation. For this turbulence model like the Standard $k-\epsilon$ and $k-\omega$ amongst others are developed. In most of the litterature the $k-\epsilon$ type of turbulence models are used. The $k-\epsilon$ models developed by Jones and Launder [1972] were further modified to improve the simulation of flows with high strain rates, improved prediction of the spreading of jets, and better results for rotational flows. The modification included a new model for the dissipation, rate ϵ and a new non-linear formulation of the eddy viscosity was introduced. The modified version of the Standard $k-\epsilon$ model is the Realizable $k-\epsilon$ model. The Standard and Realizable $k-\epsilon$ turbulence models are the most widely used in the field of biomass combustion [Dernbecher et al., 2019].
Knaus et al. [2000] investigated the application of different turbulence models used in combustion of the freeboard gas-phase for small scale wood heaters. A comparison between the Standard $k-\epsilon$ and Low Reynolds $k-\epsilon$ and Reynolds stress turbulence model was carried out for the simulation. The best agreement of simulation results and measurements were achieved by using the Low Reynolds $k-\epsilon$ model in the freeboard gas-phase combustion simulation.
Galletti et al. [2016b] compared Standard $k-\epsilon$, Realizable $k-\epsilon$ and $k-\omega$ for a wood chip with a moving grate. All three turbulence models produced acceptable results, however, the predicted CO_2 concentrations and temperature profiles from the Standard $k-\epsilon$ turbulence model were in slightly better agreement with the measurements compared to those predicted by the other turbulence models.
Farokhi et al. [2017] tested the influence of turbulence, combustion models and chemistry schemes on a small scale local biomass furnace. Simulations were carried out with the Standard k_ϵ, Realizable $k-\epsilon$ and RNG $k-\epsilon$ turbulence models. Additionally, two combustion models were testet i.e. eddy dissipation concept and steady flamelet model. In both combustion models, the RNG $k-\epsilon$ turbulence model achieved better results than the others, but the simulation results did not differ significantly from each other.

The 88MW Grate-fired Boiler EV3

3

In this chapter, the 88MW grate fired boiler, EV3 is introduced. The data, drawings, pictures are provided by Chungen Yin from the PSO report Yin [2007]. The boiler was constructed in 1997 for a maximum heat capacity of 88 MW.The maximum mass flow rate of steam produced in the boiler is 34 kg/s of steam at 557 $°C$ and 226 bar. The boiler is sketched in Figure 3.1.

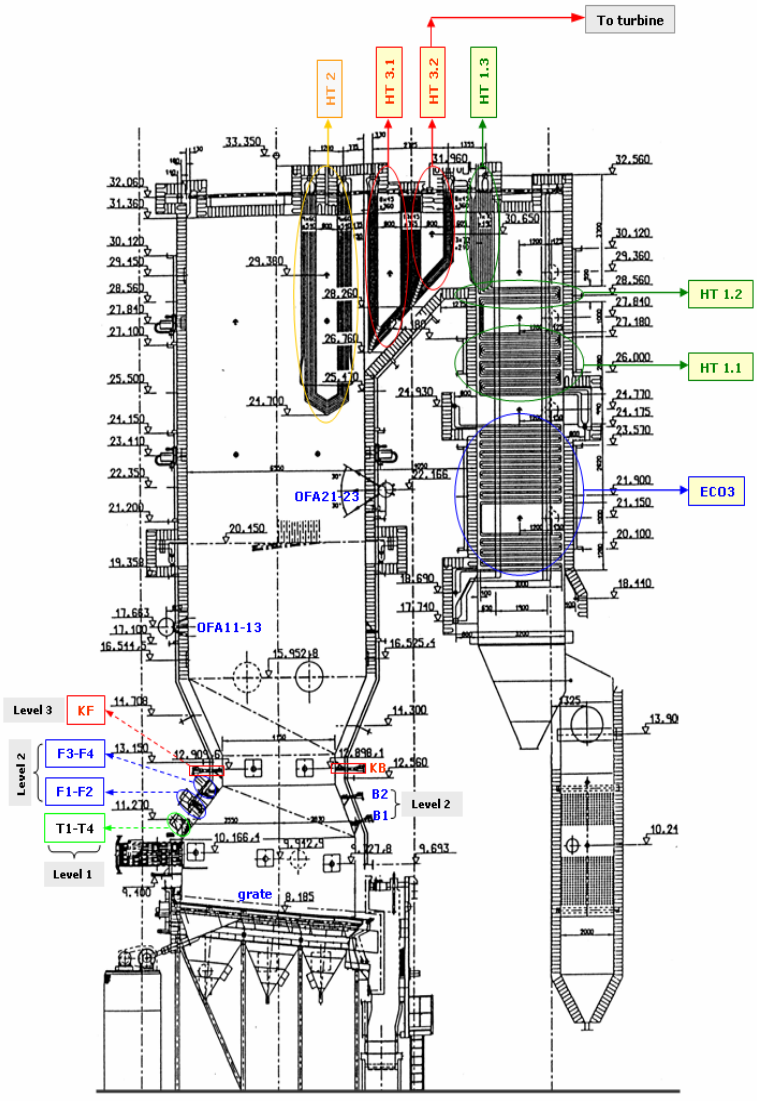

Figure 3.1: *Drawing of the boiler EV3*

As ilustrated in Figure 3.1, secondary air (SA), and overfire air (OFA) nozzles are located at different heights above the grate with different orientations and diameters. Various heating components are inside the boiler such as the super-heaters at the top and the ECO3 at the end of the computational domain of the boiler.

The boiler has four water-cooled vibrating grates located at the bottom of the combustion chamber. The grates are responsible for the transportation of the fuel from inlet to the ash discharging system, and to provide Primary Air (PA) for the conversion of the biomass in the fuel bed. The PA is provided through small holes in the grate as illustrated in the Figure 3.2.

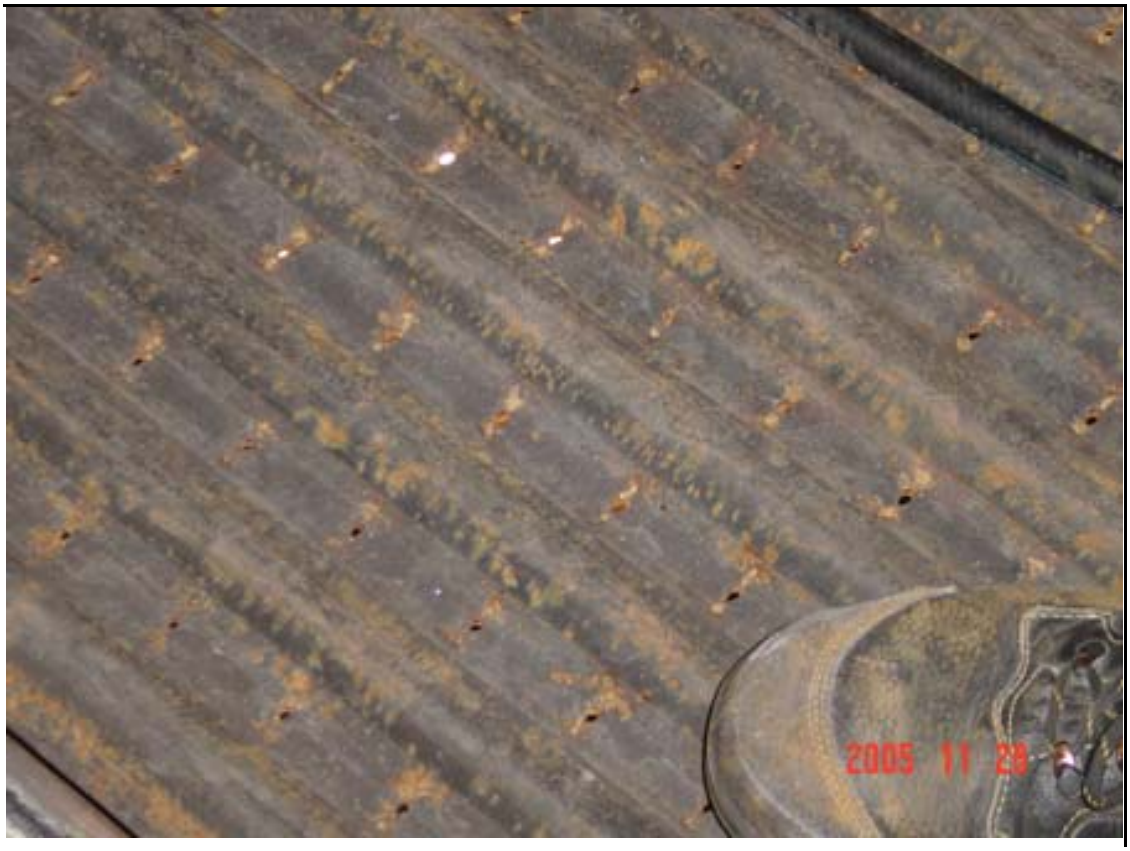

Figure 3.2: *Small holes in the grate providing PA and water tubes for cooling*

The straw inlets (totally four) on the front wall and a group of ignition air nozzles (T1-T4 in Figure 3.1) are illustrated in Figure 3.3.

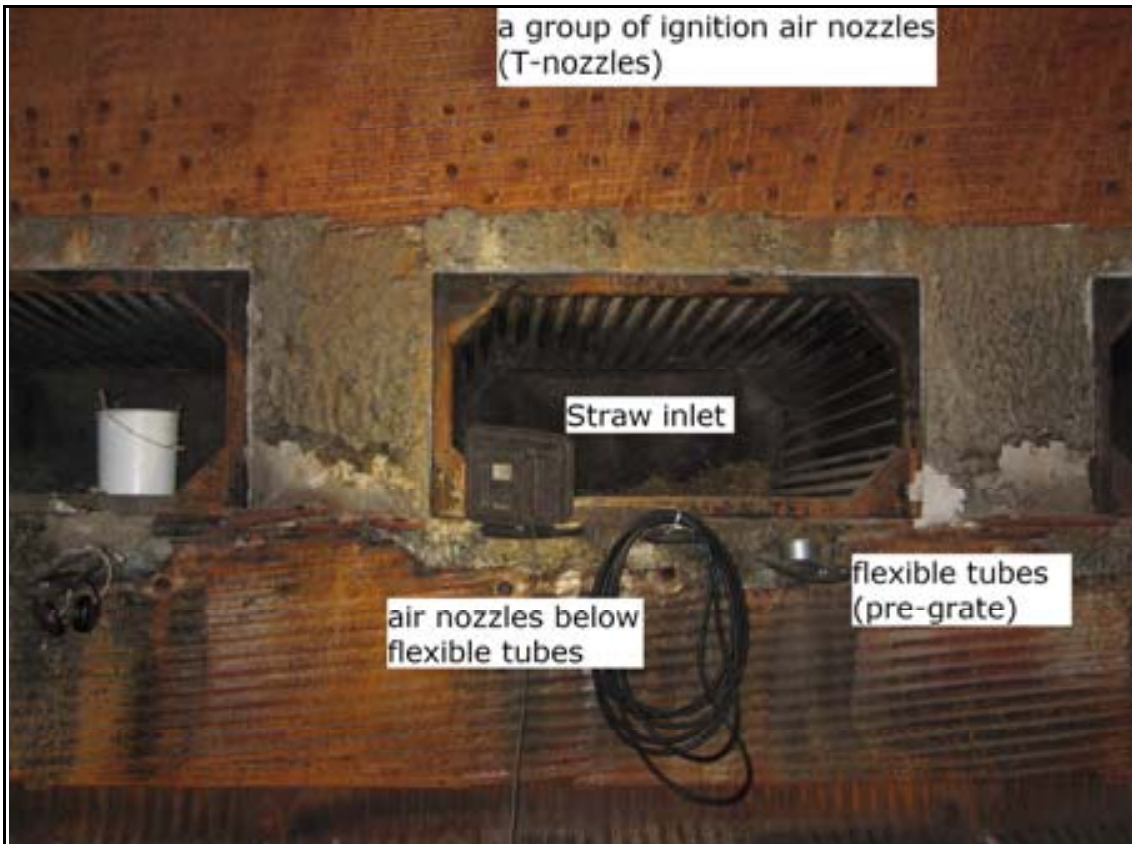

Figure 3.3: *Straw inlets with the ignition air nozzles above it on the front wall of the boiler*

3.1 Boundary conditions(BC) for the EV3 boiler

The provided data is for load 96.8 %. The data of straw chemical composition, temperature and mass flow rate is presented in Table 3.1.

Table 3.1: *Feeding rate, straw composition and temperature data for the EV3 boiler*

Property	**Unit**	**Load 96.8 %**
Feeding rate	kg/s	4.499
Temperature	°C	25
Moisture	%wt(dry)	13.4
Ash	%wt(dry)	4.5
C	%wt(dry)	47
H	%wt(dry)	5.9
N	%wt(dry)	0.7
O	%wt(dry)	41.9
Volatiles	%wt(dry)	79
Fixed Carbon	%wt(dry)	16.5
LHV	MJ/kg (AR)	14.9

The PA entering the grate is controlled by wind-boxes, therefore, the PA distribution on the grate is divided into four zones connected to their respective wind-box. The PA data is listed in Table 3.2.

Table 3.2: *PA data in the EV3 boiler*

Zone	Length [m]	PA [kg/s]
Pre-gate	0.915	2.143
1	1.403	3.287
2	2.109	3.493
3	1.953	3.235
SUM	6.38	12.158
PA temperature [K]		563.4

The SA and OFA data used in the different air nozzles are listed in Table 3.3.

Table 3.3: *SA and OFA data in the EV3 boiler*

Zone	Air Nozzles	SA & OFA [kg/s]
Ignition air (L1)	T1-T4	1.59
F-nozzles (L2)	F1-F4	1.17
Construction(L3)	KF and KB	0.62
Over-Fire Air	OFA1 and OFA2	2.13
B-nozzles (L2)	B1-B2	1.17
SUM		16.54
PA temperature [K]		563.4

The boundary condition on walls and heating surface are given in terms of temperature and emissivity. The temperature is estimated from the water/steam cycle and emissivity is adjusted for a correct heat flux. The boundary conditions of walls and heating surfaces are listed in Table 3.4 and 3.5.

Table 3.4: *Water/steam cycle inside the EV3 boiler, temperature and heat from which wall boundary conditions are determined*

Water/steam flow path inside the boiler.	Inlet T [C]	Outlet T [C]	Inlet P [bar]	Outlet P [bar]
ECO3 (counter flow)	284.3	337.5	230	229.1
Furnace Wall	337.5	390.4	229.1	215.5
Roof/HP/2nd pass walls	390.4	420.3	215.5	214.6
SH1 (counter flow)	415.2	454.7	213.7	212.9
SH2	436.6	449.5	212.0	211.1
SH3	449.5	470.0	211.1	210.2

Table 3.5: *Water/steam cycle inside the EV3 boiler, temperature and heat from which wall boundary conditions are determined*

Water/steam flow path inside the boiler.	**Inlet h [KJ/kg]**	**Outlet h [KJ/kg]**	**Mass [kg/s]**	**Heat [MW]**
ECO3 (counter flow)	1252	1546	31.89	9.376
Furnace Wall	1546	2673	31.89	35.94
Roof/HP/2nd pass walls	2673	2888	31.89	6.857
SH1 (counter flow)	2862	3055	32.39	6.251
SH2	2977	3036	33.64	1.985
SH3	3036	3120	33.64	2.826

CFD Modelling Approach for the EV3 Boiler 4

In this chapter, the general approach of modelling the EV3 boiler is presented. The simple fuel bed model procedure is outlined. Furthermore, the combustion and radiation models used in simulation of the gas-phase combustion in the freeboard are introduced. An UDF for modelling deposition in the EV3 boiler is presented. Finally, the numerical solution methods used in the CFD simulation of combustion in the EV3 boiler are outlined.

4.1 General Modelling Approach

Modeling of biomass combustion in a grate boiler involves two parts: modeling of straw conversion i.e. drying, devolatilization, char oxidation and ash formation in the fuel bed, and simulation of gas-phase reactions in the freeboard by using appropriate combustion and radiation models. The two processes are strongly coupled by the combustion gas leaving the fuel bed into the freeboard and the radiative heat flux emitted by the flame and furnace walls onto the fuel bed. The coupled modeling methodology needs to iteratively switch between the in-bed fuel conversion modeling and the freeboard CFD simulation, until there is no substantial change in either the combustion gas leaving the fuel bed or the radiative heat flux incident onto the fuel bed. The modelling approach is illustrated in Figure 4.1.

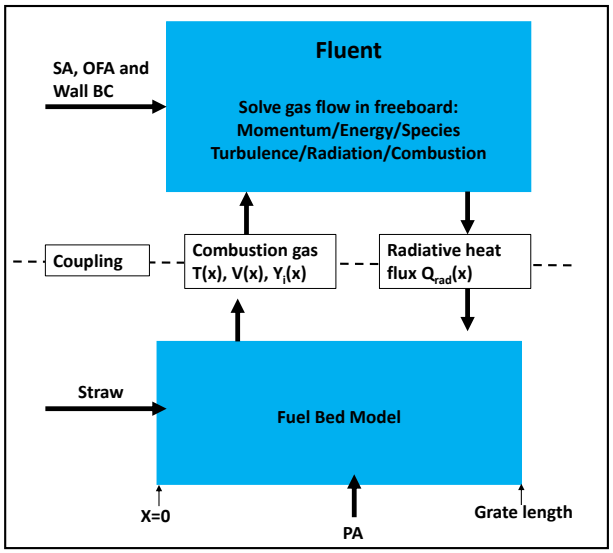

Figure 4.1: *The modelling approach used for the simulation of combustion in the EV3 boiler*

The bed model and freeboard CFD simulations are coupled by the straw leaving the fuel bed as combustion gas with a certain temperature, velocity and composition and is used as the inlet boundary condition for the gas-phase combustion simulation.The radiative heat flux from the gas-phase simulation is emitted onto the fuel bed, as illustrated in Figure 4.1.

4.2 Empirical bed model

In the field of grate-fired biomass combustion, different approaches have been made to establish a reliable bed model. From the simplest bed models being empirical bed models to fully 3D bed models. Miljković et al. [2013] developed a two-dimensional bed model for straw combustion in a moving grate. The results were compared to experimental and numerical results in the literature and there was a good agreement between the results of different processes in the moving grate. Buczyński et al. [2012] developed a time-dependent three-dimensional bed model for combustion of solid fuels in a fixed bed and good agreement with measurements were achieved. Yin et al. [2008b] investigated the effect of bed models on large-scale grate-fired boilers. CFD results based on detailed bed models were compared to the results from simple empirical bed models. The effect of the bed models were mainly restricted to the fuel bed results and the gas-phase flow pattern, gas species and temperature distribution did not show significant differences.
The bed model used in this project is a simple empirical bed model which serves the purpose of deriving the profiles of temperature, composition and velocity of gas leaving the fuel bed into the freeboard. The profiles are based on the input parameters to the fuel bed i.e. feeding rate and composition of straw, the flux of the primary air distribution and the radiative heat flux at the top of the fuel bed.

The empirical bed model calculates the straw conversion at the grate based on the lengthwise position on the grate. It is observed from measurements and experience that the straw conversion rates are a function of the position of the grate. The assumed straw conversion rates are illustrated in Figure 4.2.

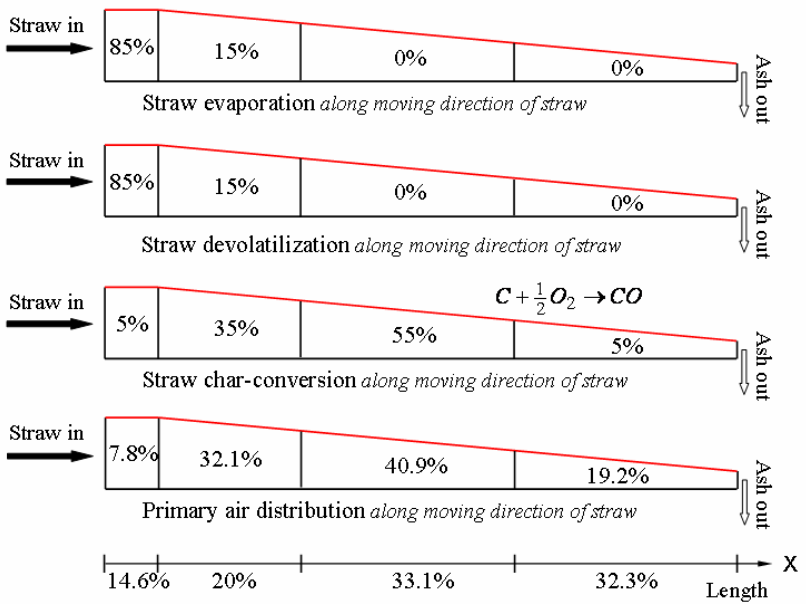

Figure 4.2: *Assumed straw conversion rates along the grate [Yin, 2007]*

The temperature, velocity and composition of the combustion gas entering the gas-phase combustion simulation are calculated from overall mass and heat balances of the three streams i.e. straw, preheated PA and the radiative heat flux.

4.3 Modelling deposition growth

Ash deposition and transport mechanisms are responsible for the ash build-up on hating surface such as the super heaters of grate-fired boilers. The ash deposition mechanism on heating surfaces are illustrated in Figure 4.3.

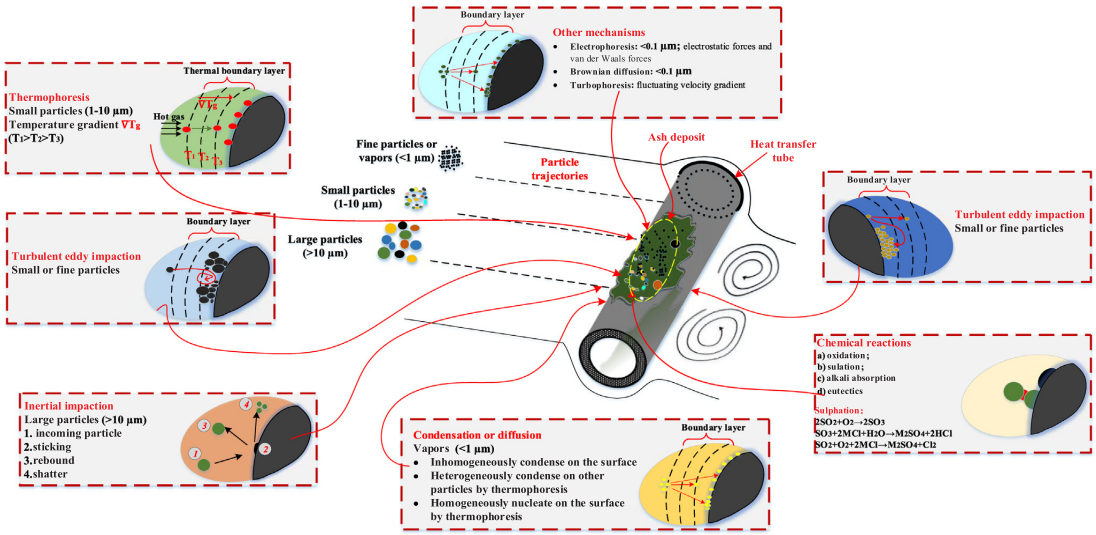

Figure 4.3: *Ash deposition mechanisms on a heat transfer tube [Cai et al., 2018]*

The mechanisms included in the deposition model are briefly explained which are inertial impaction, turbulent eddy impaction, thermophoresis and diffusion.
The most import mechanism that contributes to the ash build-up process is the inertial impaction mechanism. This mechanism is when relatively large particles ($d_p > 10\mu m$) have enough inertia to follow the gas flow and eventually collide on the heat exchange surface. The rate at which the ash particle arrives onto the heat exchange surface is proportional to the velocity of the ash particle, the particulate burden in the boiler and the impaction and capturing efficiency. If the particles are too small or light to inertially impact on the surface, turbulent eddy impacton occurs. The deposits are formed by eddies near the boundary layer. Deposits formed by turbulent eddy impaction are particularly in the back side of the heat transfer tubes or in economizers where temperature is not as high and the velocity increased When gas particle travels through the gas caused by the the temperature gradients, the thermophoretic force is generated. Hence, resulting in ash deposition by the mechanism of thermophoresis. This mechanism may become dominant in cases where the temperature difference between the flue gas and surface is large enough for submicron particles ($d_p < 10\mu m$). The deposits formed by thermophoresis are uniformly distributed around the super-heater tubes. The boundary layer temperature gradient decreases because of deposit accumulation on the surface caused by thermophoresis. Hence, the rate of thermophoresis decreases.
Initially, the deposition is controlled by diffusion due to the presence of alkali species. Diffusion occurs by the inorganic species travelling through cool heat exchange surfaces and condense on the surface or on the deposits [Cai et al., 2018].

The deposition model is developed by Kãr [2001] and Kær et al. [2006]. The model is introduced in this report. For more details, one can refer to the citation mentioned The concept of the deposition model is illustrated in the flow chart in Figure 4.4.

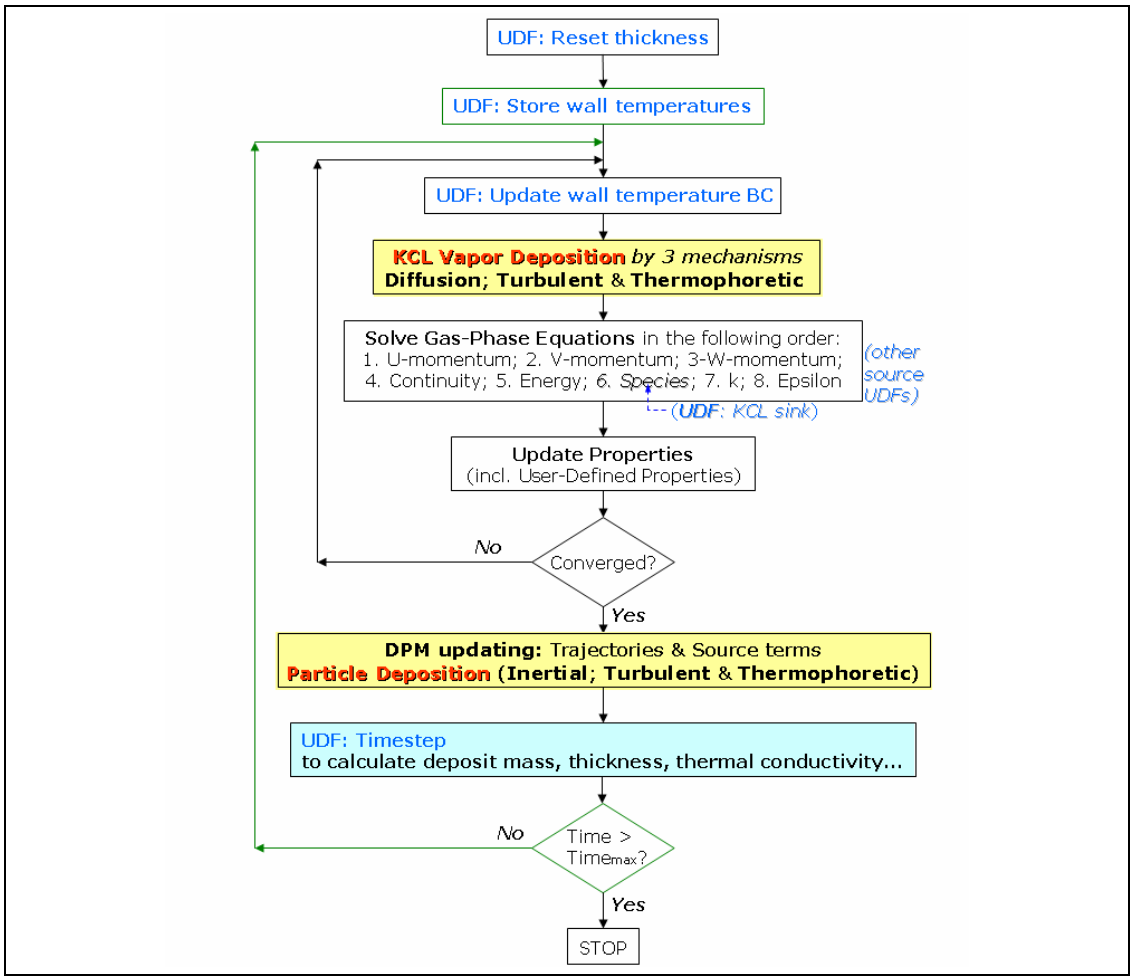

Figure 4.4: *Flowchart of the deposition model [Yin, 2007]*

The model is based on a quasi-transient approach and is integrated with the CFD simulations through a UDF. A steady-state combustion simulation provides gas composition, velocity and temperature and particle composition, velocity and temperature. Based on the converged steady-state solution, local deposit accumulation rates are calculated. The prediction is then advanced in time. Based on the time step and size and deposition rates new deposit surface conditions are estimated and these are used as new wall surface boundary conditions in the steady-state CFD combustion simulations. This iterative process is continued until the desired hours of deposit modelling is reached.

The concept of CFD based ash deposition modelling is illustrated in Figure 4.5.

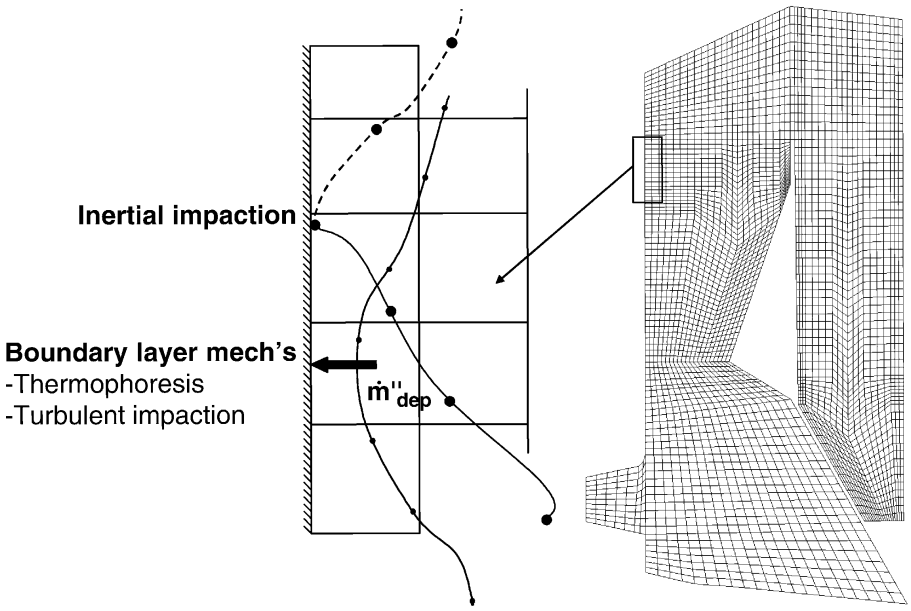

Figure 4.5: *Concept of CFD based ash deposition modelling [Kær et al., 2006].*

The concept of representing deposition by boundary layer phenomena relies on the dimensionless deposition velocity, the same idea as wall functions are used to predict shear stress, heat and mass transfer in the boundary layer. The regimes of dimensionless deposition velocity as a function of the dimensionless particle relaxation time are illustrated in Figure 4.6.

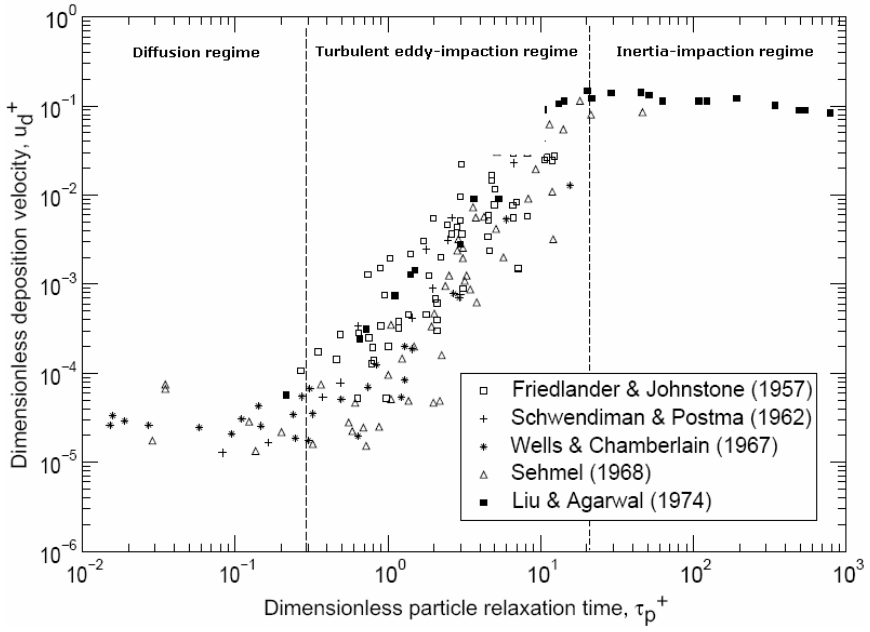

Figure 4.6: *Dimensionless deposition velocity as a function of the dimensonless particle relaxation time [Yin, 2007].*

As illustrated in Figure 4.6, diffusion is the dominant deposition mechanism

for submicron particles. For larger particle inertial impaction is the dominant mechanism for ash deposition build-up.
Deposits are build-up from fly ash particles $2 - 250\mu m$, following a certain distribution, and vapor. Only KCl vapor is considered and assumed to form submicron particle of constant size ($0.5\mu m$ in the boundary layer close to walls. Four different mechanism are considered in the model.

1. Fly ash particles: inertial, turbulent and thermophoretic mechanisms.
2. KCl vapor particles: diffusion, turbulent and thermophoretic mechanisms.

The different correlations for their corresponding mechanism are introduced and only the most relevant equations are presented.

The dimensionless deposition velocity, deposition velocity and friction velocity are given by Equation 4.1

$$u_d^+ = \frac{u_d}{u_\tau}; \qquad u_d = \frac{\dot{m}_d''}{C_0}; \qquad u_\tau = \sqrt{\frac{\tau_w}{\rho_g}} \tag{4.1}$$

The dimensionless particle velocities due to diffusion and turbulent regimes are given in Equation 4.2.

$$u_{d,Diff}^+ = 0.057 Sc_p^{-2/3}; \qquad u_{d,Turb}^+ = min(4.5 \cdot 10^{-4}(\tau_p^+)^2, \quad 0.14) \tag{4.2}$$

The Schmidt number and the dimensionless particle relaxation time is given by Equation 4.3.

$$Sc_p = \frac{\nu}{D_p} = \frac{3\pi\mu^2 d_p}{\rho_g k_B T_W C_c}; \qquad \tau_p^+ = \frac{1}{18} C_c \times S \times (d_p^+)^2 \tag{4.3}$$

The dimensionless particle deposition velocity due to thermophoresis and particle relaxation time are given in Equation 4.4.

$$u_{d,Therm}^+ = \frac{F_{therm}\tau_p}{m_p u_\tau}; \qquad \tau_p = \frac{C_c \rho_p d_p^2}{18\mu} = C_c \frac{S d_p^2}{18\nu} \tag{4.4}$$

The thermophoretic force is given in Equation 4.5.

$$F_{therm} = \frac{1.15 K_n [1 - exp(-\frac{\alpha}{K_n})](\frac{4}{3\pi}\phi\pi_1 K_n)^{0.5})\frac{K_B}{d_m^2} d_p^2 \nabla T}{4\sqrt{2}(1 + \frac{\pi_1}{2} K_n)} \tag{4.5}$$

The Knudsen number, α, temperature gradient, ϕ_1 and molecular diameter are given in Equaiton 4.6 and Equation 4.7.

$$K_n = \frac{2\lambda}{d_p}; \qquad \alpha = 0.22\left[\frac{\frac{\pi}{6}\phi}{1+\frac{\pi_1}{2}K_n}\right]^{0.5}; \qquad \nabla T = \frac{q_{conv}}{k_{gas}A_{conv}} \tag{4.6}$$

$$\pi_1 = 0.5816; \qquad d_m = (\frac{5}{16\mu})^{1/2}(\frac{M \cdot k_B \cdot T_g}{\pi})^{1/4} \tag{4.7}$$

The total deposition KCl is given in Equation 4.8.

$$\dot{m}''_{d,KCl\ vapor} = \underbrace{(u^+_{d,Diff} + u^+_{d,Turb} + u^+_{d,Therm}) \cdot u_\tau}_{Total\ KCl\ deposition\ velocity,\ u^+_{d,KCl}} \times \underbrace{(\rho_{gas} \cdot Y_{KCl})}_{Local\ KCl\ vapor\ mass\ concentration} \tag{4.8}$$

The total deposition of fly ash is given i Equation 4.9.

$$\dot{m}''_{d,DPM} = \frac{\dot{m}_p \eta_{stick}/A}{\dot{m}''_{d,inert}} + \frac{(u^+_{d,Turb} + u^+_{d,therm})u_\tau \cdot Conc_p \cdot \eta_{stick}}{\dot{m}''_{d,Turb} + \dot{m}''_{d,Therm}} \tag{4.9}$$

The net fraction of particles contributing to deposit growth is given by Equation 4.10.

$$\eta_{stick} = \underbrace{p(T_p)}_{Particles} + \underbrace{(1 - p(T_p)p(T_w))}_{Deposit\ surface} \tag{4.10}$$

$$p(T_P) = \begin{cases} 0 & \text{if } T_p < T_{stick} \\ 1 - \frac{T_{stick2} - T_P}{T_{stick2} - T_{stick1}} & \text{if } T_{stick1} < T_P < T_{stick2} \\ 1 & \text{if } T_p > T_{stick2} \end{cases} \tag{4.11}$$

$$p(T_w) = \begin{cases} 0 & \text{if } f_{melt}(T, Y_i) < 0.1 \\ \frac{f_{melt}(T,Y_i) - 0.1}{0.6} & \text{if } 0.1 < f_{melt}(T, Y_i) < 0.7 \\ 1 & \text{if } f_{melt}(T, Y_i) > 0.7 \end{cases} \tag{4.12}$$

The temperature dependency of the melt fractions are determined from Figure 4.7.

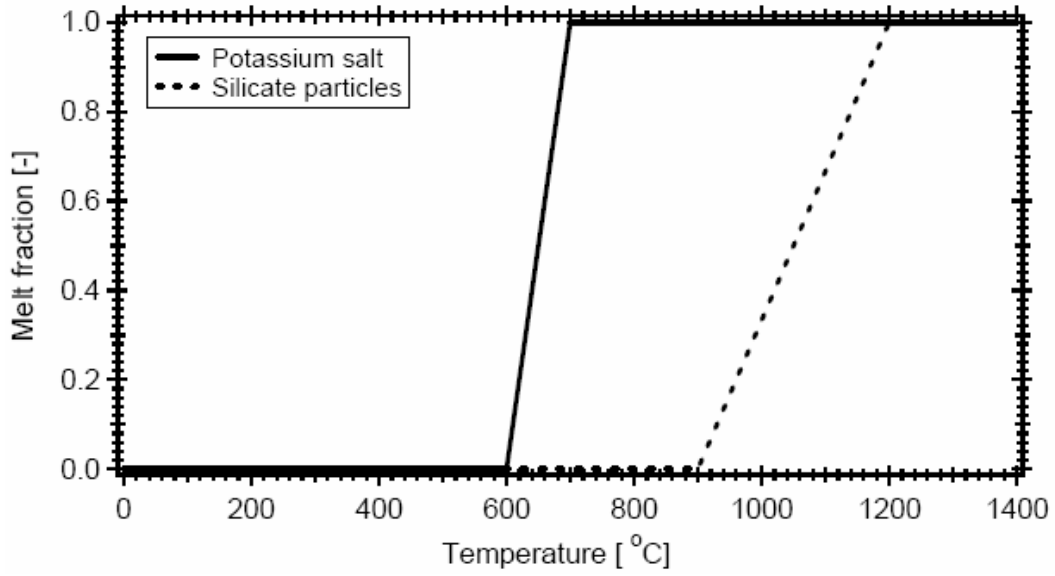

Figure 4.7: *Approximated melting curves of potassium salt silicate particles [Yin, 2007].*

The sum of the deposition rates of KCl and fly ash is the total deposition rate given by Equation 4.13.

$$\dot{m}_d'' = \dot{m}_{d,KCl\ vapor}'' + \dot{m}_{d,DPM}'' \tag{4.13}$$

4.4 Combustion and radiation models and numerical solution methods used in the simulation of the EV3 boiler

The finite rate/eddy dissipation model is used to solve the gas-phase turbulence-chemistry interactions with a two step global reaction mechanism where CO is the intermediate. The finite rate/eddy dissipation calculates both the Arrhenius rate and Eddy dissipation rate and uses the lower of the two. A general problem with this model is the overpredicted flame peak temperature due to the chemistry only being described by a two-step global reaction mechanism without accounting for the intermediate species or the dissociation effects occuring at high temperatures. The default values of the constants A (4) and B (0.5) used in calculating the combustion rate in the Eddy dissipation model could be too high. Therefore, the values used in this report are A=0.6 and B=0.5 as proposed by Yin et al. [2008b] amongst others.

Heat transfer by radiation is modelled using the discrete ordinate radiaton model (DOM). This model requires specification of the angular resolution for which the radiative transfer equations (RTE) are solved. The angular resolution used in the

simulations is $2 \times 2 \times 8 = 32$ discrete directions.

The numerical solution methods and settings set in Fluent® are given in Table 4.1.

Table 4.1: *Solution methods, convergence criteria, turbulence models and discretization schemes used in the simulations.*

Solution methods	**Used in simulations**	**Turbulence model and convergence criteria**	**Used in simulations**
Scheme	SIMPLE	Turbulence model	Realizable k-ϵ
Gradients	Green-Gauss Cell Based	Wall functions	Standard wall functions
Pressure	Standard	Continuity	1E-3
Momentum	First Order Upwind		
Continuity	First Order Upwind	Energy	1E-6
Energy	First Order Upwind		
Species	First Order Upwind	x,y,z-velocities	1E-3
k and ϵ	First Order Upwind	Species	1E-3
DO	First Order Upwind	k and ϵ	1E-3

CFD Results and Data Validation 5

In this chapter, the results from the CFD simulations are presented. Four cross sections are selected to present the results from the CFD simulation and these are compared to measured data. Various contour plots are examined to illustrate the temperature, species and velocity distribution in the EV3 boiler. Finally, examples of the deposition mechanism involved in combustion are outlined from contour plots. Initially, mesh quality checks and the overall heat and mass balance is presented.

5.1 Mesh quality and overall heat and mass balance

The computational domain is discretized into decent volumes and shapes in order to solve the algebraic form of the transport equations. Hence, it is of importance to ensure the quality of the mesh in order to obtain grid independent solutions and ensure convergence and physical realistic solutions. The mesh generated for the EV3 boiler is provided by Chungen Yin. It purely consists of 3822540 hexahedral cells. The mesh quality is investigated through different mesh quality checks. In this case, two properties are investigated, as illustrated in Figure 5.1.

Figure 5.1a illustrates the equiangle skewness of the mesh. This is a measure of how close to ideal a face or cell is. A value of zero corresponds to a complete equiangular cell and that is the best in terms of quality. A value of 1 is a degenerate cell. ANSYS® Academic Fluent®, Release 19.2 Users Guide states that a skewness below 0.75 is fair to use [ANSYS, 2018]. Most of the cells in the mesh have skewness close to zero, however, some relatively skewed cells are located around the grate, air nozzles and super-heaters. Nevertheless, these are few cells and the overall quality of the mesh in terms of skewness is considered to be very good. Figure 5.1b shows the smoothness i.e. volume change between neighbouring cells. If the smoothness exceeds five, the cells are considered to be poor. If the smoothness is between 1 and 2.5, the cells are considered to be very good[ANSYS, 2018]. Most of the cells are below 2.5 with some exceptions located near the grate, air nozzles and super heaters. In overall, the mesh is considered to be good in terms of the mentioned quality checks.

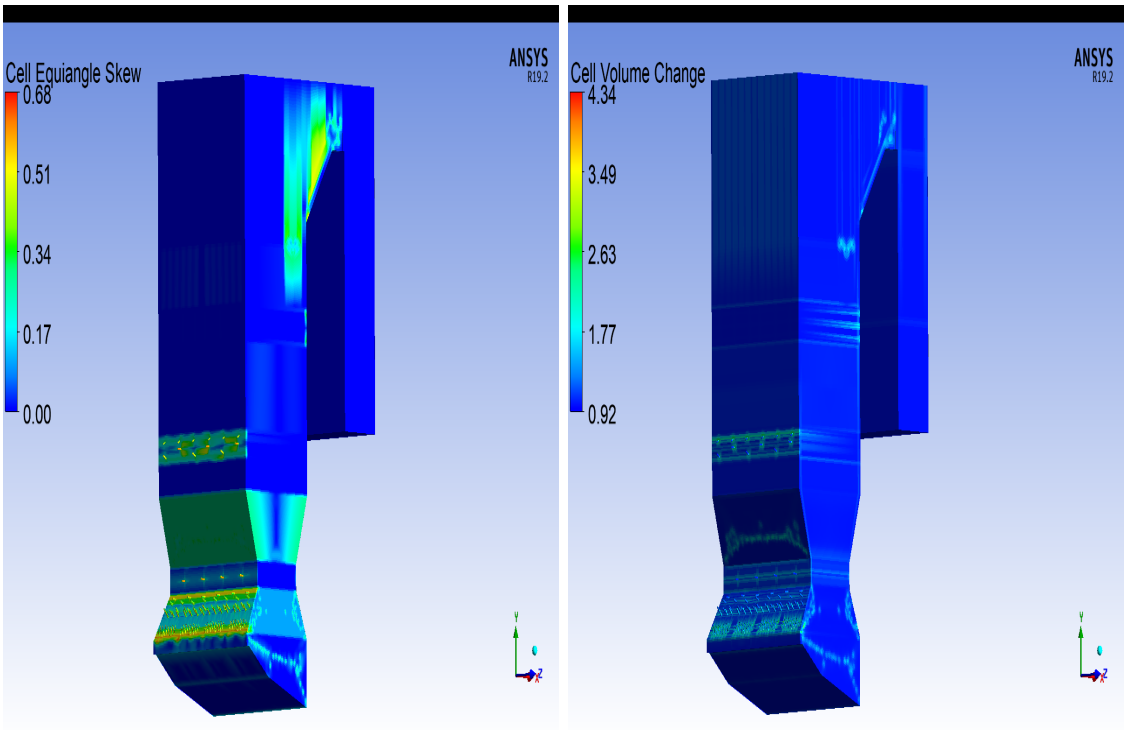

(a) *Equiangle skewness of the entire computational domain*

(b) *Cell volume change of the entire computational domain*

Figure 5.1: *Selected mesh quality checks for the the entire computational domain of the EV3 boiler*

It is important to verify that mass and energy are conserved for any CFD problem, regardless of the discretization and solution methods used. Table 5.1 shows the heat and mass balance of the EV3 boiler model.

Table 5.1: *Mass and heat transer rates*

Property	Model input	Model output	Deviation
Heat Transfer Rate [MW]	83.07	83.08	0.01 %
Mass Transer Rate [kg/s]	33.04	33.04	0.00%

Table 5.1 shows that mass and heat is conserved with a tiny deviation on the heat transfer rate. The results from the simulation of combustion in the EV3 boiler and measurements are presented.

5.2 Data validation

The measuring ports on the EV3 boiler are illustrated in Figure 5.2. The measured data is provided by Sønnik and Ejvind, and the data corresponds to five different ports in the EV3 boiler i.e. port E,F,G,H and I. Ejvind only provided measurement data for port F and for the rest of the ports only Sønnik's data is available. Port

E and F lies on the same horizontal line as indicated by Figure 5.2. Therefore, a horizontal plane on this line is chosen to present relevant data from the simulations. Furthermore, the ports G,H and I lies on the same horizontal line, hence another plane is chosen to present CFD data at this level. Additionally, two vertical planes at different locations are selected to present relevant results from the CFD simulations of combustion of biomass in the EV3 boiler.

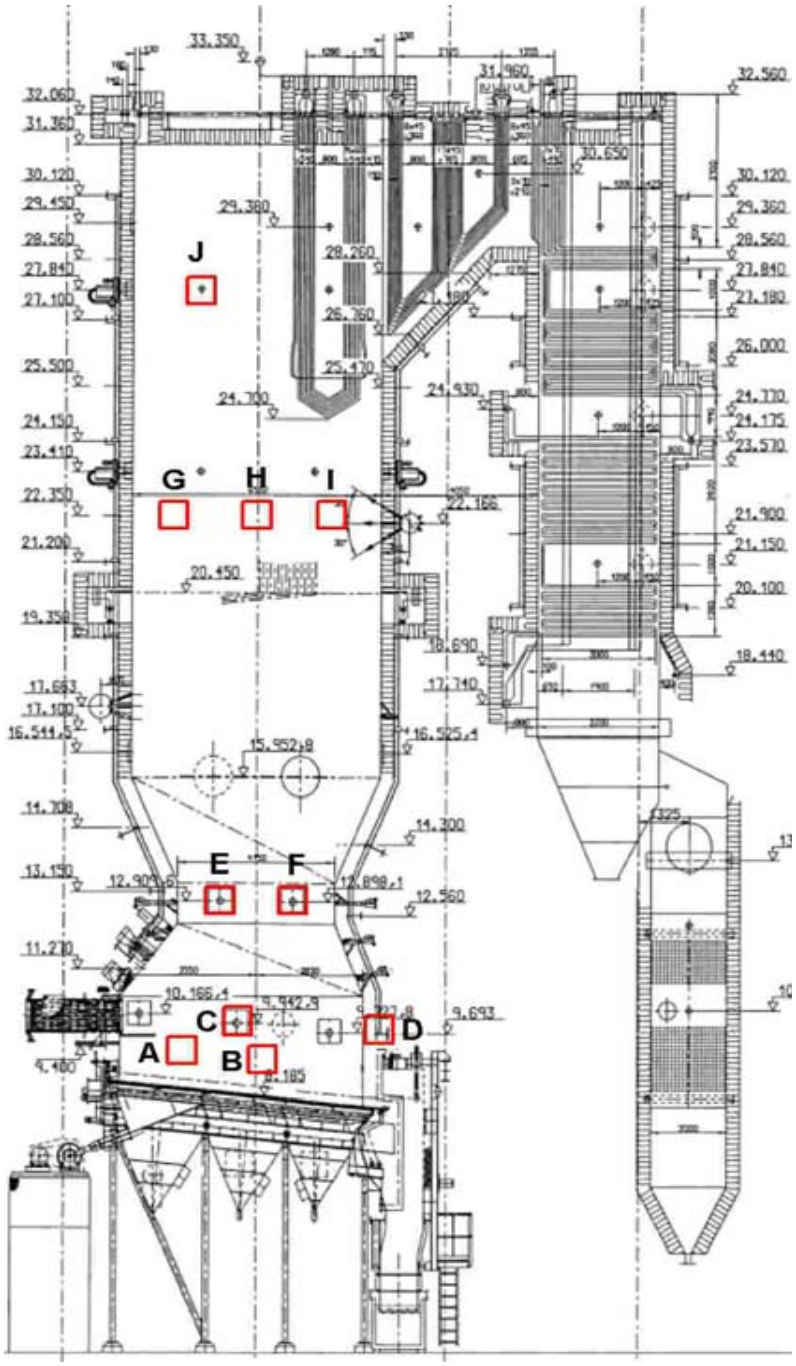

Figure 5.2: *Measuring ports in the EV3 boiler [Yin, 2007].*

The locations of the chosen cross sections in the EV3 boiler are illustrated in Figure 5.3.

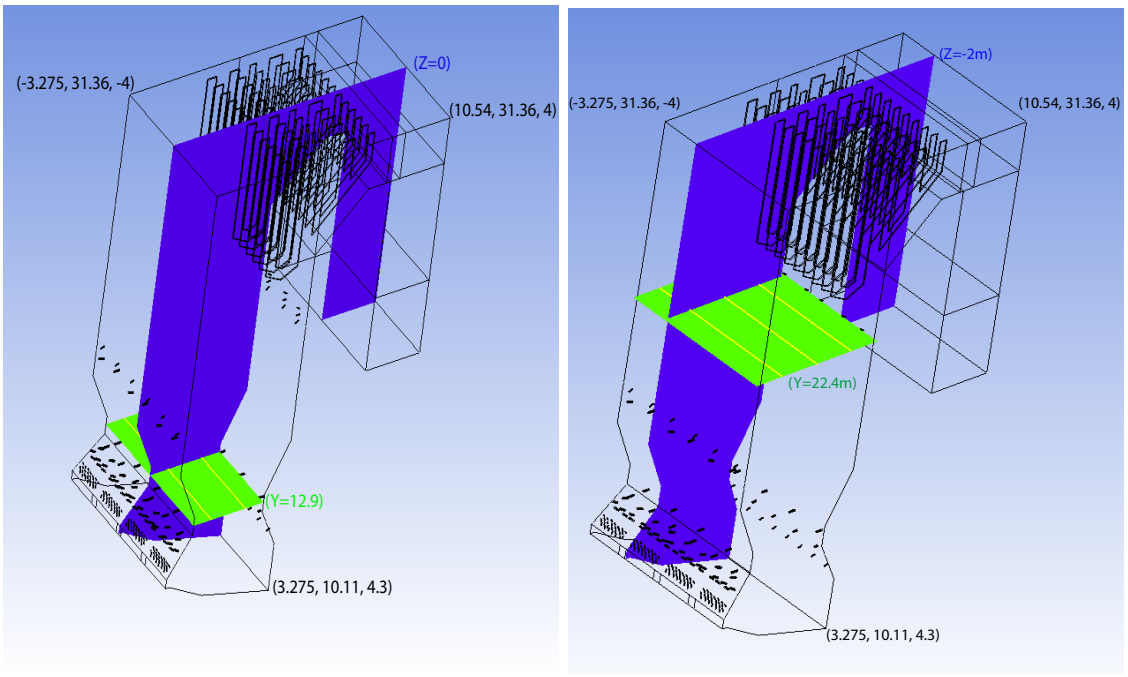

(a) *Cross sectional plane at Z=0 [m], and horizontal plane at the two measuring ports E and F*

(b) *Cross sectional plane at Z=-2 [m], and horizontal plane at the three measuring ports G, H and I*

Figure 5.3: *The location of the four planes where the CFD results are shown and the yellow line indicates the location of the five measurement ports i.e. E,F,G,H and I*

The results from the simulation and the provided data for temperature and some chemical species are plotted in Figure 5.4 to Figure 5.8.

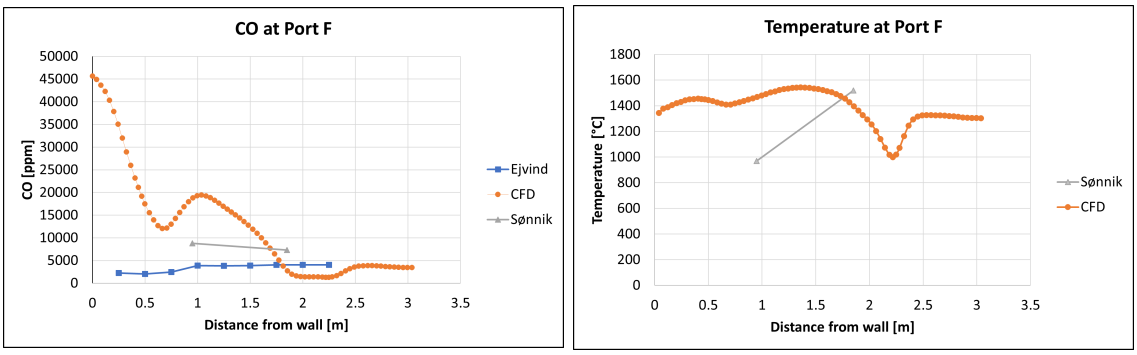

(a) **(b)**

Figure 5.4: *CO and Temperature at Port F*

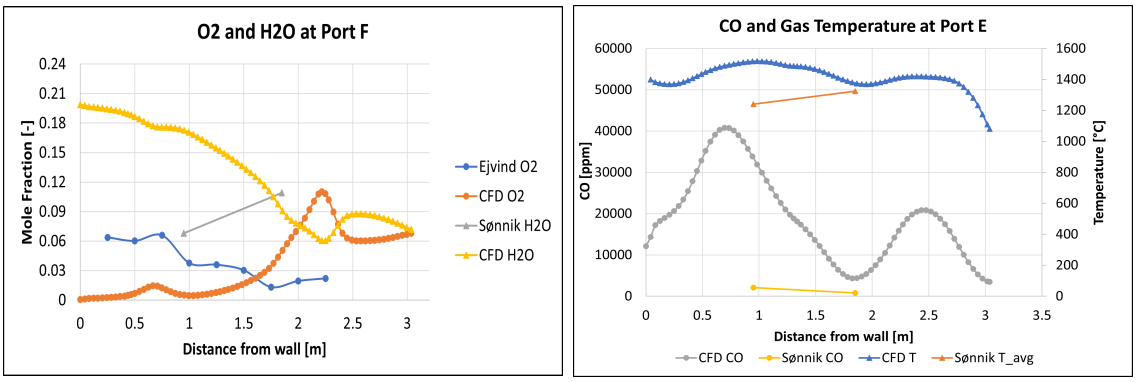

(a) (b)

Figure 5.5: *(a):O_2 and H_2O at port F, (b): CO and temperature at port E*

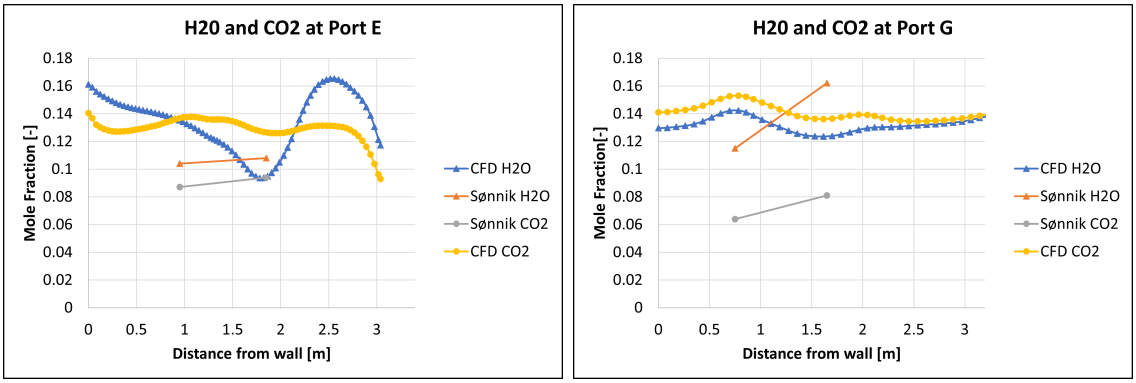

(a) (b)

Figure 5.6: *H_2O and CO_2 at port E (a) and port G (b)*

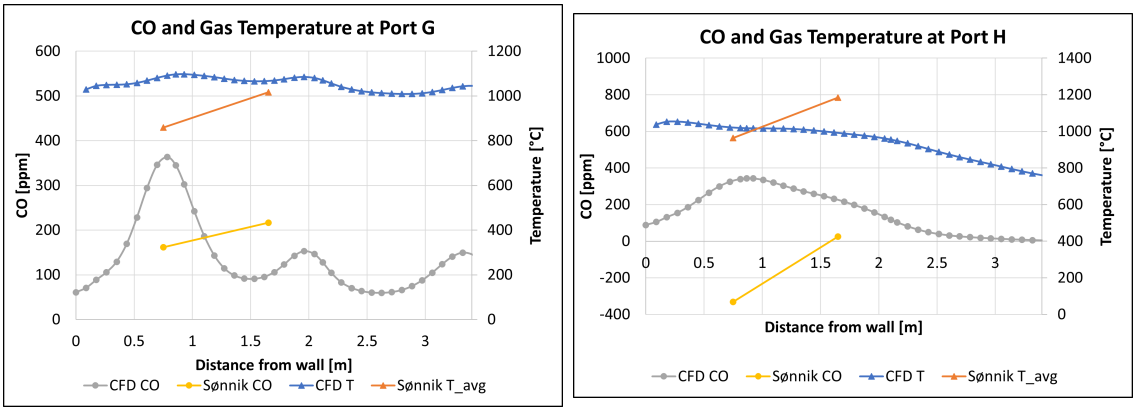

(a) (b)

Figure 5.7: *CO and Temperature at Port G (a) and port H (b)*

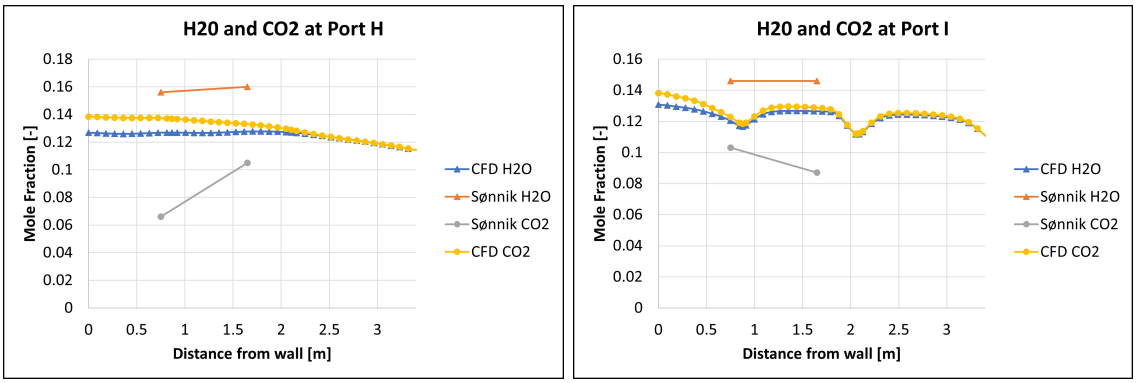

(a) **(b)**

Figure 5.8: *H_2O and CO_2 at port H (a) and port I (b)*

The data from measurements and CFD simulations is presented in Figure 5.4-5.8. As seen on Figure 5.4 (a), the measured data from Ejvind deviates considerably from the measured data of Sønnik. This could be caused by different measuring techniques used for respectively Ejvind's and Sønnik's measurements. Possibly, the measurements are done at different times which might explain the difference in the measured data. There is a significant difference between the measured data of the five measuring ports i.e. F,E,G,H and I and the results from the CFD simulations on the same ports. The discrepancy is for all of the five measuring points and both for gas temperature and chemical species. The gas temperature data from Sønnik is averaged (he provided minimum and maximum temperature) and the plot illustrates the average temperature. This is done because the range of the minimum and maximum temperature was relatively small compared to the scale of the graphs. Therefore, the graphs for minimum and maximum temperature would overlap each other. It should be noted that the measured CO content at port H 5.7b (b) is negative which is not possible, this might be a mistake.

One of the reasons for the significant discrepancy between the measurements and results from the CFD simulations might be that the boundary conditions used in CFD does not represent the real boundary conditions in the boiler under operation from which the measurements are carried out. In large-scale grate furnaces combustion disturbances are a common phenomena, which causes non-uniform distribution of air and thus un-even fuel conversion at the grate[Duffy, 2012]. Therefore, the boundary conditions from the bed model to the freeboard gas-phase CFD simulations could deviate significantly from the real ones.

Another reason is that in the CFD simulation the effect of deposition on the boiler is neglected. Especially, in the regions around air nozzles, the orientation of the incoming air jets might be changed because of deposition. Hence, the boundary conditions from the inlet air nozzles might not be accurate when deposition is not taken into account.

In overall, the bad agreement between the CFD results and the measurements are due to the lack of accounting for deposition, the occurrence of non-uniform feeding

rates and combustion disturbances - meaning that results from the CFD model are based on an ideal case and the measurements are from a real boiler.

5.3 Contour plots

The contour plots of the four mentioned cross sections are examined. These are illustrated in Figure 5.9 - 5.16.

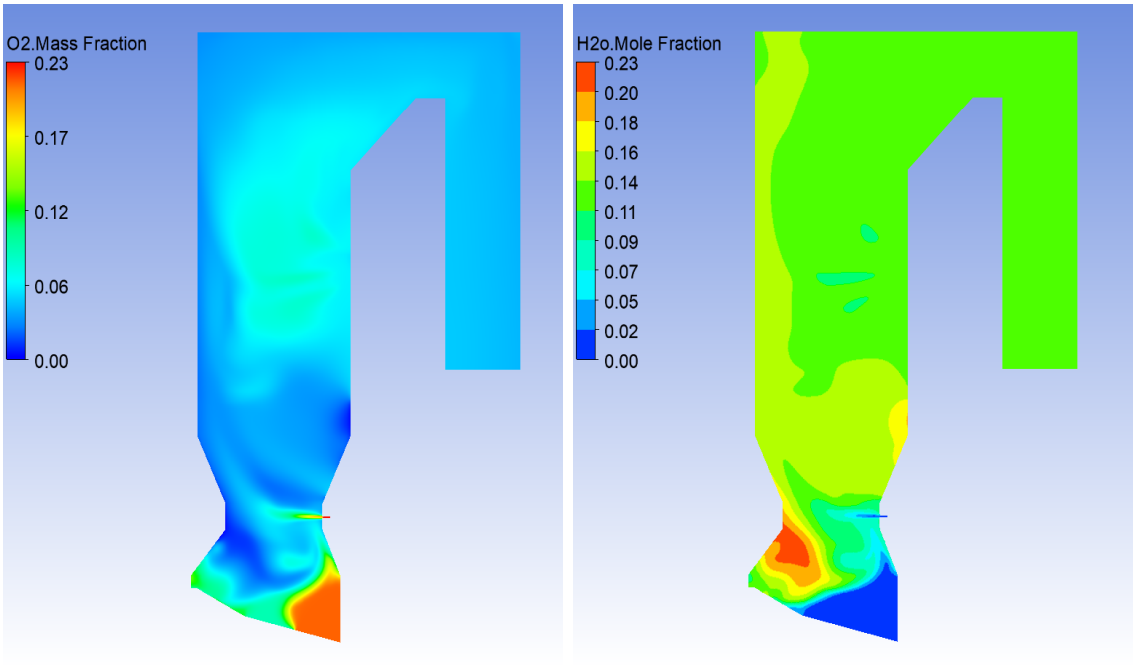

(a) **(b)**

Figure 5.9: *$O_2(a)$ and $H_2O(b)$ contours at plane Z=0 [m]*

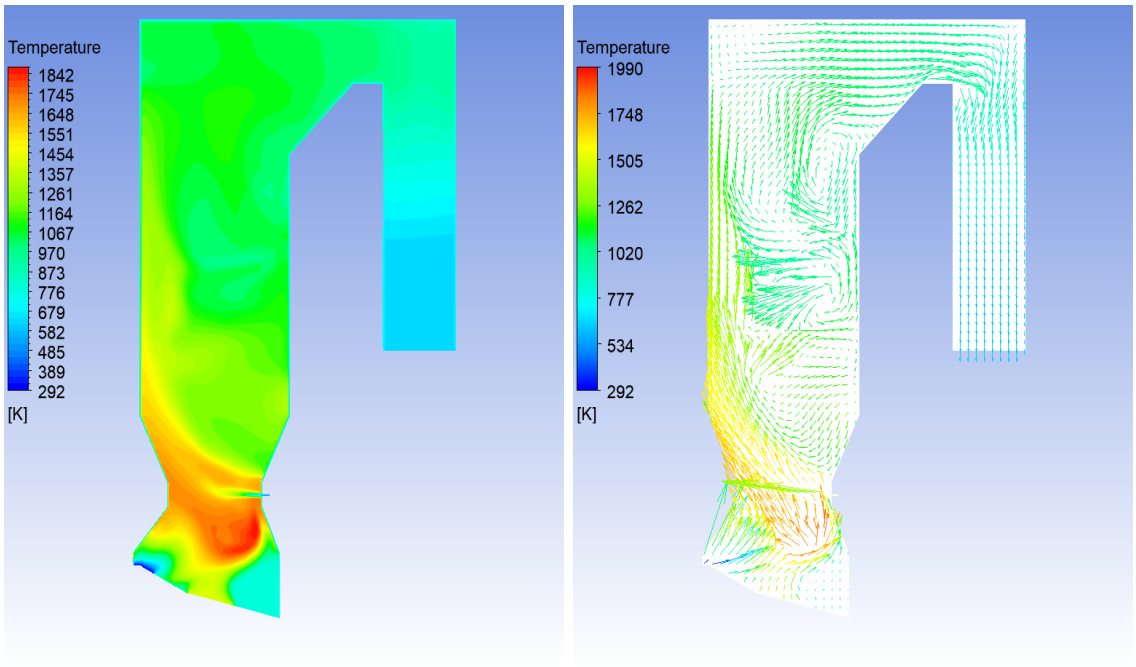

(a) **(b)**

Figure 5.10: *Temperature(a) and Velocity vectors coloured by temperature(b) contours at plane Z=0 [m]*

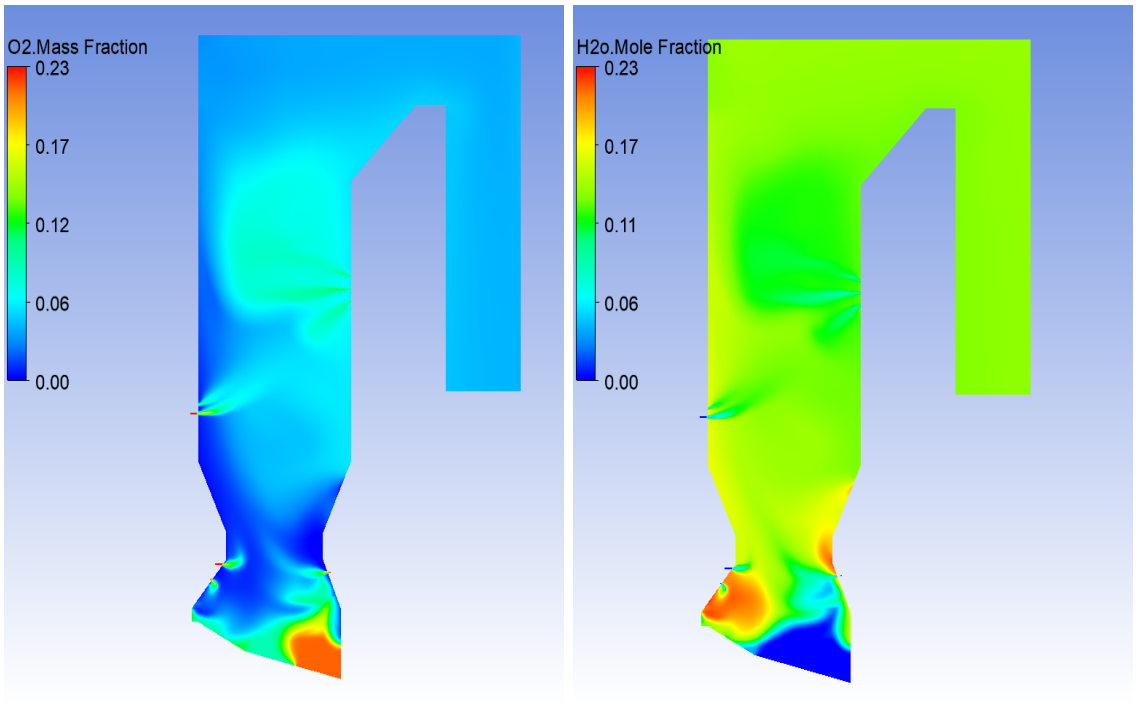

(a) **(b)**

Figure 5.11: *O_2(a) and H_2O(b) contours at plane Z=-2 [m]*

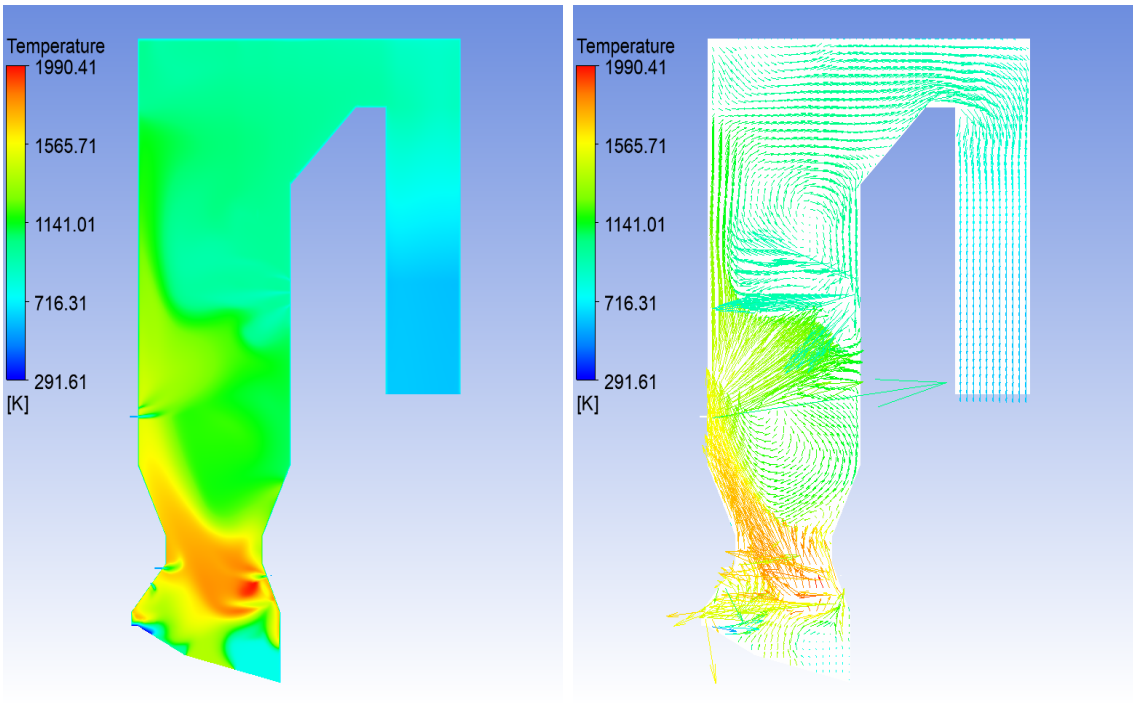

(a) **(b)**

Figure 5.12: *Temperature(a) and Velocity vectors coloured by temperature(b) contours at plane Z=-2 [m]*

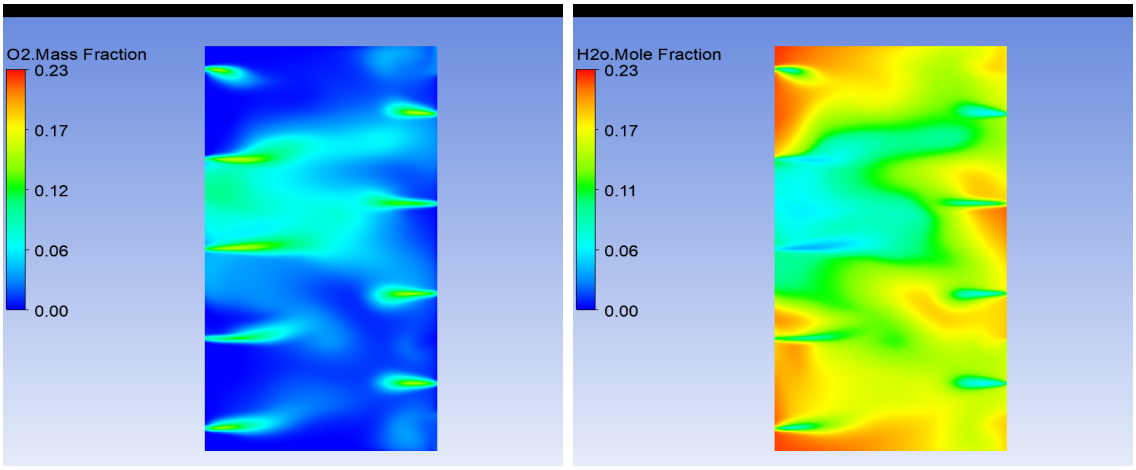

(a) **(b)**

Figure 5.13: *O_2(a) and H_2O(b) contours at horizontal plane at Y=12.9 [m]*

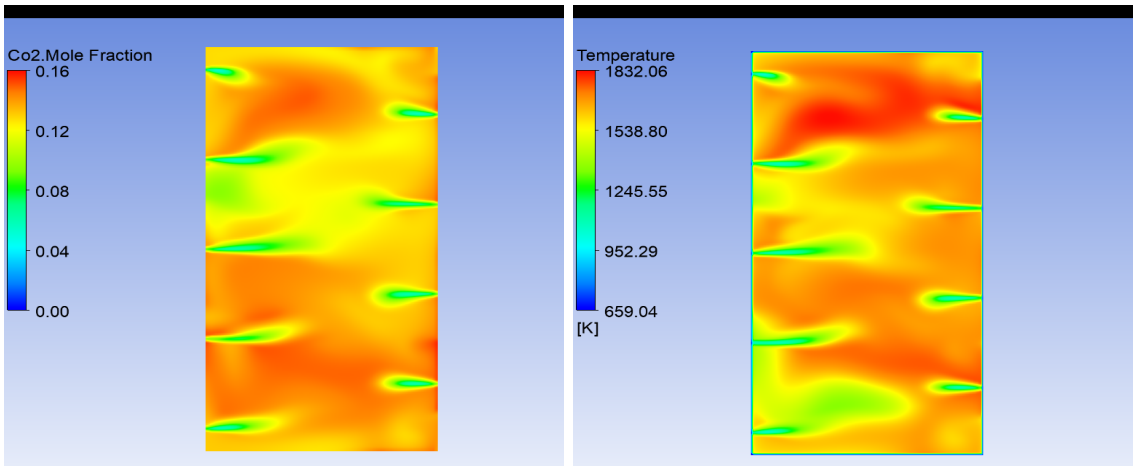

(a) **(b)**

Figure 5.14: *CO_2(a) and Temperature(b) contours at horizontal plane at Y=12.9 [m]*

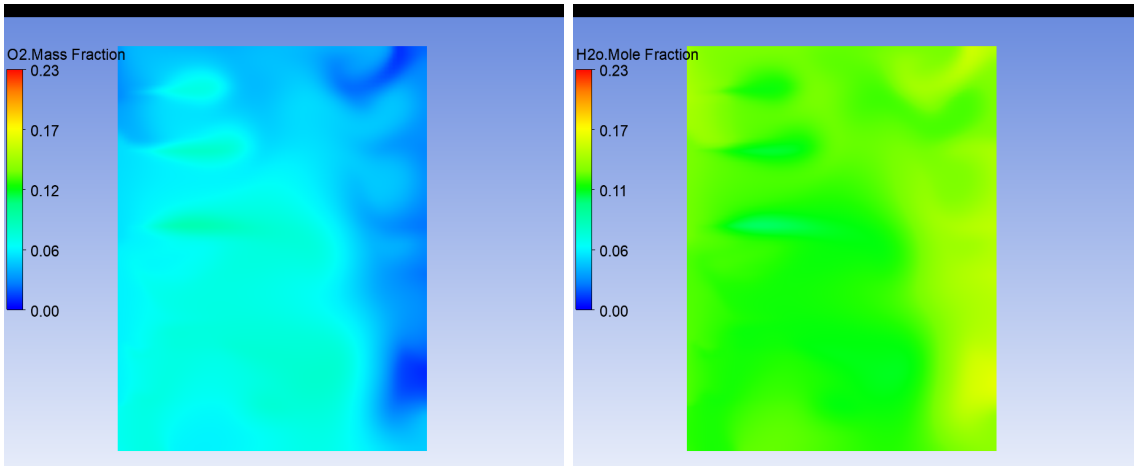

(a) **(b)**

Figure 5.15: *O_2(a) and H_2O(b) contours at horizontal plane at Y=22.4 [m]*

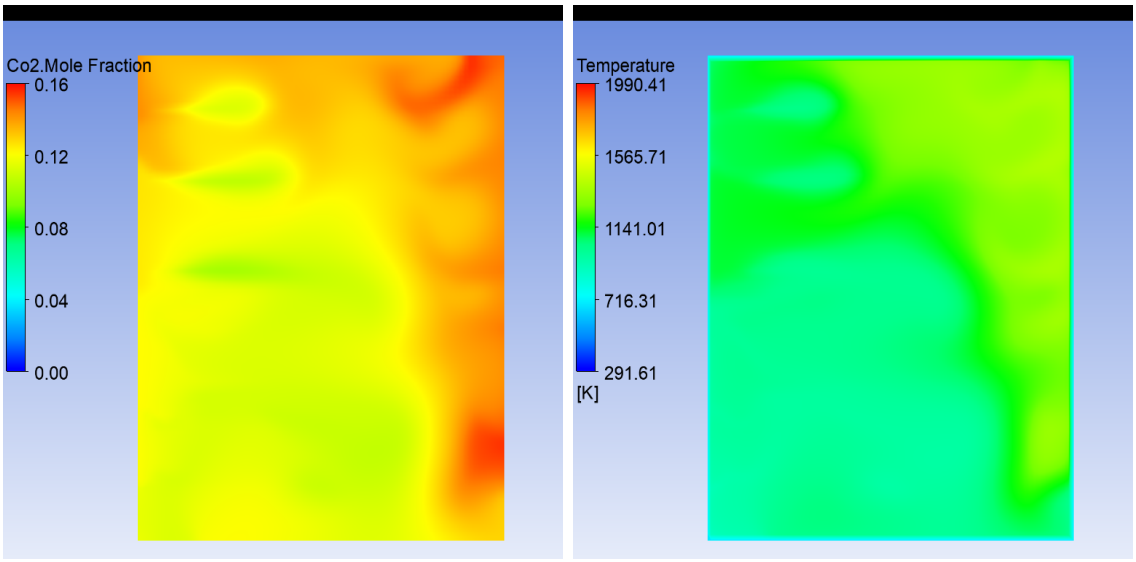

(a) **(b)**

Figure 5.16: *CO_2(a) and Temperature(b) contours at horizontal plane at Y=22.4 [m]*

The velocity vectors contour in Figure 5.10b and 5.12b indicates that two local recirculation zones exist in the center of the boiler. These recirculation zones enhance mixing in the boiler and thereby combustion. Mixing of air and volatile biomass is very crucial to combustion, thus the placement of the air nozzles and primary air distribution should be thoroughly considered in the design phase of the boiler. Furthermore, the vector plots indicates that the radiation shaft is fully utilized and the main flow is not confined to a specific location of the radiation shaft.
It is observed from Figure 5.10a and 5.12a that the primary combustion zone is relatively close to the grate which may increase the uncertainties in determining the species concentration and temperature profile at the bed top.
Figure 5.9a and 5.11a, shows that the O_2 level at the end of the grate is relatively high. The primary air distribution along the grate can be adjusted to account for this unwanted high level of O_2.
The horizontal planes at $Y = [12.9[m]$ in Figure 5.13 and 5.14 indicates that mixing in this region could be improved. Large variations in temperature and chemical species are present. The data comparison between the measurements and CFD results was partly from this horizontal plane. If the measurement and CFD results are not obtained for exactly the same location, large deviation between the measurements and CFD results will be observed. However, the horizontal planes at $Y = 22.4[m]$ in Figure 5.15 and 5.16 shows more appropriate mixing.

5.4 Deposition contours

The deposition model was not succesfully implemented in the combustion simulation of the EV3 boiler. However, this deposition model was implemented on another boiler by Chungen Yin. Chungen Yin provided simulation results. The contours are from his simulation of the deposition model. Contours are created from the simulation in order to show some of the mechanisms of deposition and understand the importance of these. The contour plot in Figure 5.17.

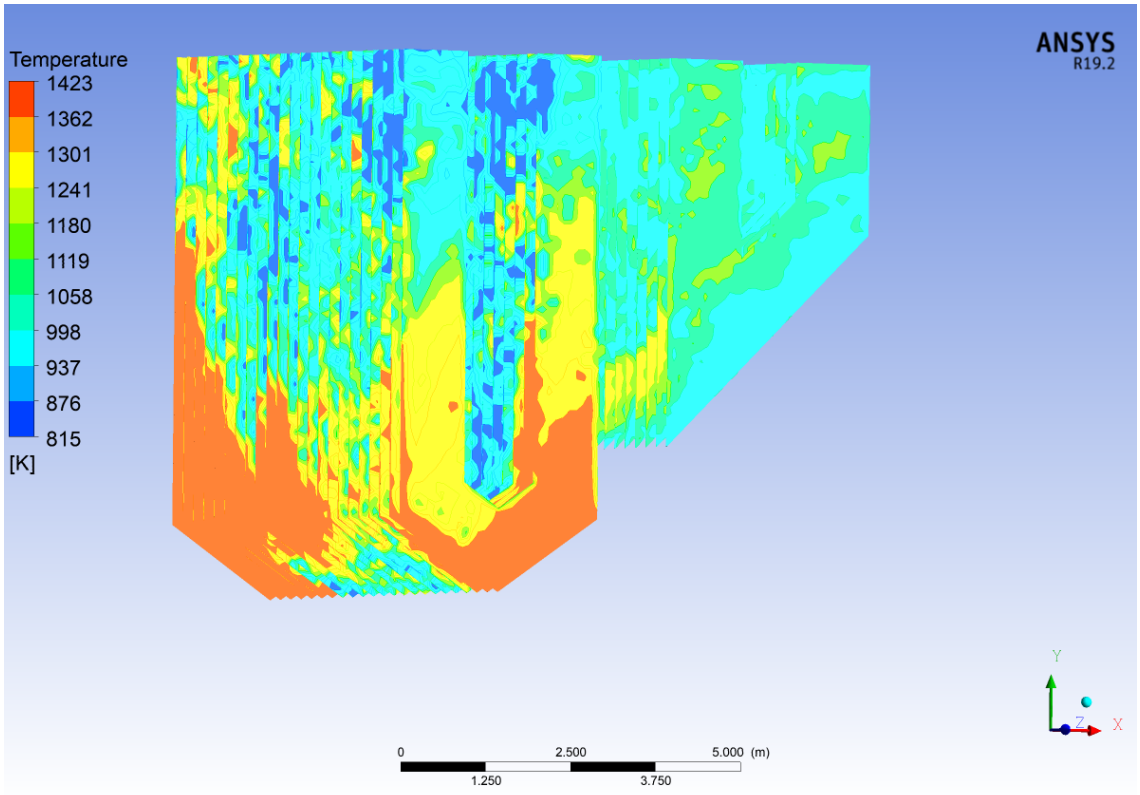

Figure 5.17: *Surface temperature [K] contours of the super-heaters after 24 hours deposit growth*

The surface temperature of the clean superheaters was uniform in respectively the first and second superheater. After 24 hours of deposition operation, the temperature is observed to increase especially at the corners of the superheaters mostly due to inertal impaction, as observed in Figure 5.17.

In order to investigate the effect of the different deposition mechanism, contours of the mass deposit fluxes at the superheater surfaces are illustrated in Figure 5.18-5.19.

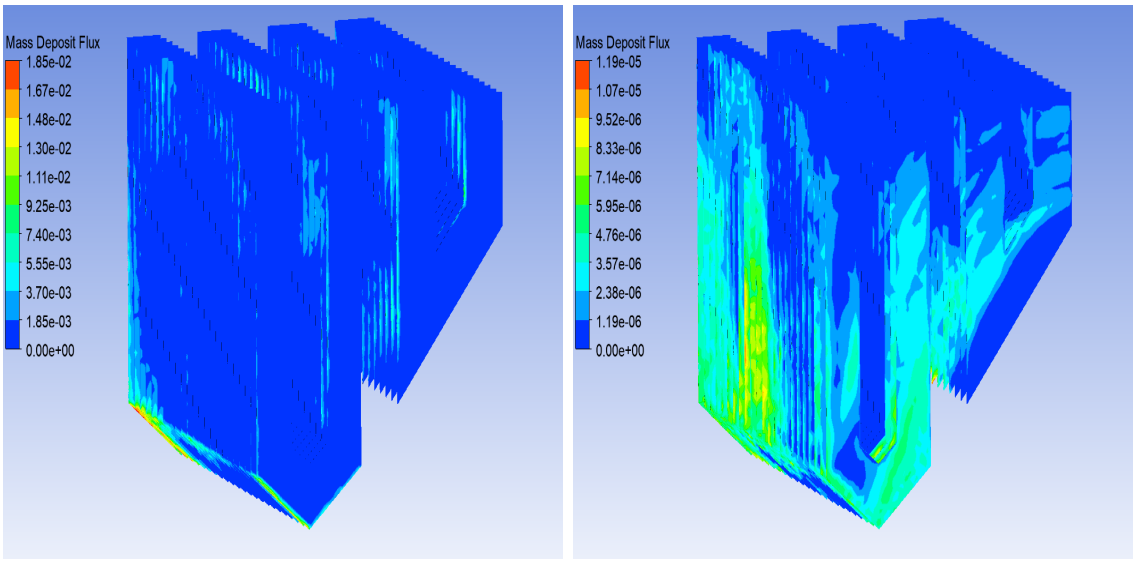

(a) **(b)**

Figure 5.18: *Inertial impaction [(a) and themophoresis (b) at the superheater surfaces after 24 hours of deposition growth in* $[kgm^{-2}s^{-1}]$

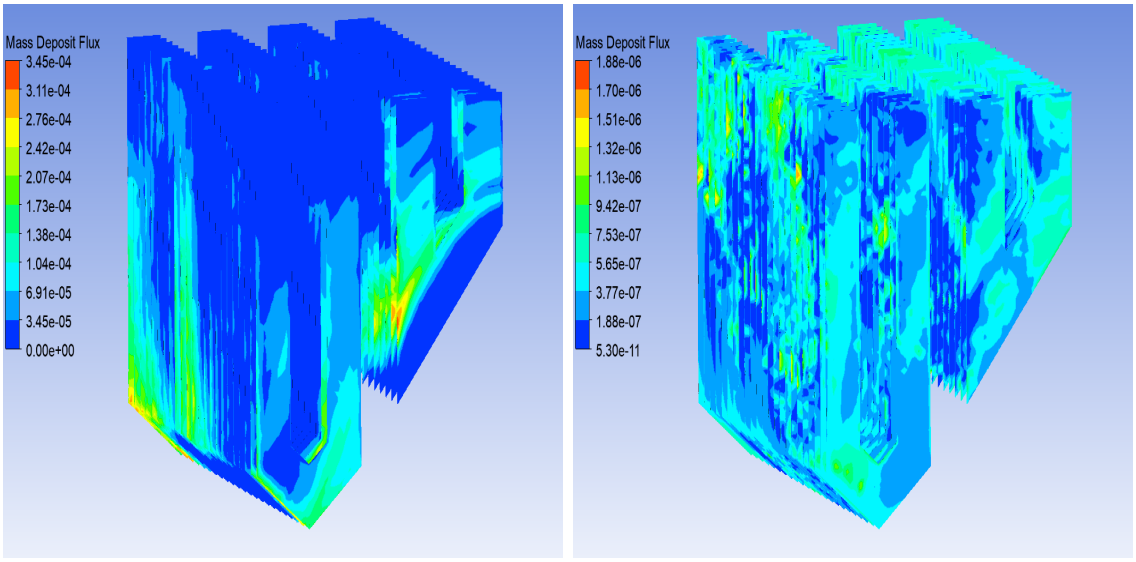

(a) **(b)**

Figure 5.19: *Turbophoresis (a) and vapor deposition (b) at the superheater surfaces after 24 hours of deposition growth in* $[kgm^{-2}s^{-1}]$

It is clearly observed from the scales in Figure 5.18 and Figure 5.19 that the dominant deposition mechanism is the inertial impaction.

Conclusion 6

The modelling approach used to model combustion in the 88MW biomass grate-fired boiler consists of two parts: modelling the straw conversion in the fuel bed and simulation of the gas-phase combustion in the freeboard. A simple empirical model was used for the in-bed fuel conversion. This model calculated the temperature, velocity and composition of the gas leaving the fuel bed into the freeboard. The simple empirical model assumes some fixed straw conversion rates along the length of the grate and these converison rates are based on measurements and experience. The temperature, velocity and gas composition leaving the fuel bed were used as boundary conditions for the gas-phase combustion simulation together with wall boundary conditions calculated from the water/steam cycle in the EV3 boiler. The deposition growth model was not successfully implemented in the EV3 boiler simulations, however, results from another case, provided by Chungen yin, were presented to outline some of the deposition mechanism and their effect on superheaters in grate-fired boilers. It was observed that the temperatures, especially at the corner of the super-heaters were high due to deposition growth . The results from simulation of combustion in the EV3 boiler were compared to measurements. The results deviated considerably from the measurements. The main reason for the discrepancies between the simulation results and measurements is that the CFD simulations were based on a clean boiler geometry and the measurements are from a boiler in operation. The boundary conditions used in the freeboard combustion simulations might not represent the real boundary conditions of the boiler since combustion disturbances were not accounted for and these are a common phenomena in large-scale boilers. Furthermore, deposition is not accounted for in the CFD simulations. Deposition accumulation is especially important in the regions near the air nozzles, since the orientation and momentum of the incoming air jets can be changed because of deposition. Velocity contour of the gas-phase combustion showed two local recirculation zones which enhances mixing in the boiler. The primary combustion zone was relatively close to the grate surface which might increase the uncertainties in determining the species concentration and temperature profiles at the bed top. Furthermore, the primary air distribution might be adjusted to avoid the unwanted high level of air at the end of the grate.

Bibliography

ANSYS, **August 2018**. ANSYS. *ANSYS Fluent User's Guide*, 2018.

Borello et al., **2013**. Domenico Borello, Paolo Venturini, Franco Rispoli and Saavedra G. Z. Rafael. *Prediction of multiphase combustion and ash deposition within a biomass furnace*. Applied Energy, 101, 413–422, 2013. doi: https://doi.org/10.1016/j.apenergy.2012.04.031. URL `http://www.sciencedirect.com/science/article/pii/S0306261912003170`. ID: 271429.

Buczyński et al., **2012**. Rafał Buczyński, Roman Weber, Andrzej Szlek and Radovan Nosek. *Time-Dependent Combustion of Solid Fuels in a Fixed-Bed: Measurements and Mathematical Modeling*. Energy Fuels, 26(8), 4767–4774, 2012. doi: 10.1021/ef300676r. URL `https://doi.org/10.1021/ef300676r`. doi: 10.1021/ef300676r.

Buczyński et al., **2015**. Rafał Buczyński, Roman Weber and Andrzej Szlęk. *Innovative design solutions for small-scale domestic boilers: Combustion improvements using a CFD-based mathematical model*. Journal of the Energy Institute, 88(1), 53–63, 2015. doi: https://doi.org/10.1016/j.joei.2014.04.006. URL `http://www.sciencedirect.com/science/article/pii/S1743967114000610`. ID: 306191.

Cai et al., **2018**. Yongtie Cai, Kunlin Tay, Zhimin Zheng, Wenming Yang, Hui Wang, Guang Zeng, Zhiwang Li, Siah Keng Boon and Prabakaran Subbaiah. *Modeling of ash formation and deposition processes in coal and biomass fired boilers: A comprehensive review*. Applied Energy, 230, 1447–1544, 2018. doi: https://doi.org/10.1016/j.apenergy.2018.08.084. URL `http://www.sciencedirect.com/science/article/pii/S0306261918312194`. ID: 271429.

Dernbecher et al., **Feb 25, 2019**. Andrea Dernbecher, Alba Dieguez-Alonso, Andreas Ortwein and Fouzi Tabet. *Review on modelling approaches based on computational fluid dynamics for biomass combustion systems*. Biomass Conversion and Biorefinery, 9(1), 129–182, 2019. doi: 10.1007/s13399-019-00370-z. URL `https://search.datacite.org/works/10.1007/s13399-019-00370-z`.

Duffy, **Dec 12, 2012**. Neil Duffy. *Investigation of Biomass Combustion in Grate Furnaces using CFD*, 2012. URL

https://explore.openaire.eu/search/publication?articleId=od_____
_1513::97380725ddeebab44454c8d8e03d19cf.

Dörrenbächer et al., 2017. Christoph Dörrenbächer, Mike Geppert, Daniel Pastuh and Matthias Tomendal. *Final report.* The European Worker Participation Competence Centre (EWPCC) of the European Trade Unions Institute (ETUI), Brussels, 2017.

Farokhi et al., 2017. Mohammadreza Farokhi, Madjid Birouk and Fouzi Tabet. *A computational study of a small-scale biomass burner: The influence of chemistry, turbulence and combustion sub-models.* Energy Conversion and Management, 143, 203–217, 2017. doi: https://doi.org/10.1016/j.enconman.2017.03.086. URL http://www.sciencedirect.com/science/article/pii/S0196890417303047. ID: 271098.

Galletti et al., 2016a. Chiara Galletti, Valentina Giomo, Simone Giorgetti, Paolo Leoni and Leonardo Tognotti. *Biomass furnace for externally fired gas turbine: Development and validation of the numerical model.* Applied Thermal Engineering, 96, 372–384, 2016. doi: https://doi.org/10.1016/j.applthermaleng.2015.11.085. URL http://www.sciencedirect.com/science/article/pii/S1359431115013319. ID: 271641.

Galletti et al., 2016b. Chiara Galletti, Valentina Giomo, Simone Giorgetti, Paolo Leoni and Leonardo Tognotti. *Biomass furnace for externally fired gas turbine: Development and validation of the numerical model.* Applied Thermal Engineering, 96, 372–384, 2016. doi: https://doi.org/10.1016/j.applthermaleng.2015.11.085. URL http://www.sciencedirect.com/science/article/pii/S1359431115013319. ID: 271641.

Jones and Launder, 1972. W. P. Jones and B. E. Launder. *The prediction of laminarization with a two-equation model of turbulence.* International Journal of Heat and Mass Transfer, 15(2), 301–314, 1972. doi: https://doi.org/10.1016/0017-9310(72)90076-2. URL http://www.sciencedirect.com/science/article/pii/0017931072900762. ID: 271451.

Jones and Lindstedt, 1988. W. P. Jones and R. P. Lindstedt. *Global reaction schemes for hydrocarbon combustion.* Combustion and Flame, 73(3), 233–249, 1988. doi: https://doi.org/10.1016/0010-2180(88)90021-1. URL http://www.sciencedirect.com/science/article/pii/0010218088900211. ID: 271463.

Karim and Jamal. M. R. Karim and Naser Jamal. *Conference Paper: Progress in Numerical Modelling of Packed Bed Biomass Combustion.*

Klason et al., **2008**. T. Klason, X. S. Bai, M. Bahador, T. K. Nilsson and B. Sundén. *Investigation of radiative heat transfer in fixed bed biomass furnaces.* Fuel, 87(10), 2141–2153, 2008. doi: https://doi.org/10.1016/j.fuel.2007.11.016. URL http://www.sciencedirect.com/science/article/pii/S0016236107005157. ID: 271496.

Knaus et al., **2000**. H. Knaus, S. Richter, S. Unterberger, U. Schnell, H. Maier and K. R. G. Hein. *On the application of different turbulence models for the computation of fluid flow and combustion processes in small scale wood heaters.* Experimental Thermal and Fluid Science, 21(1), 99–108, 2000. doi: https://doi.org/10.1016/S0894-1777(99)00059-X. URL http://www.sciencedirect.com/science/article/pii/S089417779900059X. ID: 271092.

Koppejan and van Loo, **2008**. Jaap Koppejan and Sjaak van Loo. *The Handbook of Biomass Combustion and Co-firing.* Routledge Ltd, London, 2008. ISBN 1849711046. doi: 10.4324/9781849773041. URL https://www.taylorfrancis.com/books/9781136553783.

Kãr, **2001**. Sãren Kãr. *Numerical investigation of ash deposition in straw-fired boilers : using CFD as the framework for slagging and fouling predictions : Ph. D. thesis.* Aalborg University Institute of Energy Technology, Aalborg, 2001. ISBN 978-87-89179-39-1.

Kær et al., **2006**. S. K. Kær, L. A. Rosendahl and L. L. Baxter. *Towards a CFD-based mechanistic deposit formation model for straw-fired boilers.* Fuel, 85 (5), 833–848, 2006. doi: https://doi.org/10.1016/j.fuel.2005.08.016. URL http://www.sciencedirect.com/science/article/pii/S0016236105002814. ID: 271496.

Miljković et al., **2013**. Biljana Miljković, Ivan Pešenjanski and Marija Vićević. *Mathematical modelling of straw combustion in a moving bed combustor: A two dimensional approach.* Fuel, 104, 351–364, 2013. doi: https://doi.org/10.1016/j.fuel.2012.08.017. URL http://www.sciencedirect.com/science/article/pii/S0016236112006539. ID: 271496.

WESTBROOK and DRYER, **1981**. CHARLES K. WESTBROOK and FREDERICK L. DRYER. *Simplified Reaction Mechanisms for the Oxidation of Hydrocarbon Fuels in Flames.* null, 27(1-2), 31–43, 1981. doi: 10.1080/00102208108946970. URL https://doi.org/10.1080/00102208108946970. doi: 10.1080/00102208108946970.

Yin, **2007**. Chungen Yin. *Grate Firing of Biomass Measurements, Validation and Demonstration*, Institute of Energy Technology, AAU, 2007.

Yin et al., 2008a. Chungen Yin, Lasse Rosendahl, Søren K. Kær, Sønnik Clausen, Søren L. Hvid and Torben Hille. *Mathematical Modeling and Experimental Study of Biomass Combustion in a Thermal 108 MW Grate-Fired Boiler*. Energy Fuels, 22(2), 1380–1390, 2008. doi: 10.1021/ef700689r. URL https://doi.org/10.1021/ef700689r. doi: 10.1021/ef700689r.

Yin et al., 2008b. Chungen Yin, Lasse Rosendahl, Søren K. Kær, Sønnik Clausen, Søren L. Hvid and Torben Hille. *Mathematical Modeling and Experimental Study of Biomass Combustion in a Thermal 108 MW Grate-Fired Boiler*. Energy Fuels, 22(2), 1380–1390, 2008. doi: 10.1021/ef700689r. URL https://doi.org/10.1021/ef700689r. doi: 10.1021/ef700689r.

Yin et al., 2008c. Chungen Yin, Lasse A. Rosendahl and Søren K. Kær. *Grate-firing of biomass for heat and power production*. Progress in Energy and Combustion Science, 34(6), 725–754, 2008. doi: https://doi.org/10.1016/j.pecs.2008.05.002. URL http://www.sciencedirect.com/science/article/pii/S0360128508000245. ID: 271467.

Yin et al., 2010. Chungen Yin, Søren K. Kær, Lasse Rosendahl and Søren L. Hvid. *Co-firing straw with coal in a swirl-stabilized dual-feed burner: Modelling and experimental validation*. Bioresource technology, 101(11), 4169–4178, 2010. doi: https://doi.org/10.1016/j.biortech.2010.01.018. URL http://www.sciencedirect.com/science/article/pii/S0960852410000751. ID: 271433.

Yongtie et al., 2018. Cai Yongtie, Tay Kunlin, Zheng Zhimin, Yang Wenming and Wang Hui. *Modeling of ash formation and deposition processes in coal and biomass fired boilers: A comprehensive review*. Applied Energy Volume 230, 230 (10), 1447–1544, 2018. URL http://www.sciencedirect.com/science/article/pii/S0306261918312194.